AACHENER VERFAHRENSTECHNIK

RWTH Aachen · AVT.**CVT** · 52064 Aachen
Chemische Verfahrenstechnik
Prof. Dr.-Ing. Matthias Wessling

ITBA · Buenos Aires, Argentina
Departamento Ingeniería Química

Decontamination of water: Adsorption of heavy metals to hematite particles, derived from Ferroxane, and a comparison of different filtration process designs

September 2014

Supervision:
Prof. As. Dra. María Marta Fidalgo
(University of Missouri, USA)
Prof. As. Mg. Liliana María Bertini
(ITBA Buenos Aires)
Prof. Dr.-Ing. Matthias Wessling
(RWTH Aachen)

Master's Thesis

Frank Bühler
Matrikel Nr.: 290286

Aachen, WS 2014/15

STATUTORY DECLARATION

I declare that I have authored this thesis independently, that I have not used other than the declared sources / resources, and that I have explicitly marked all material which has been quoted either literally or by content from the used sources.

date signature

Contents

List of Figures

List of Tables

1 Introduction

The presence of heavy metal ions in water poses a major environmental health risk to local residents.[1] Industrial waste water often contains heavy metal ions, e.g., chromium, lead and nickel. If the waste water is not properly treated prior to discharge, these highly toxic metal ions may leak into the ground water.[2]

A warning example is the highly contaminated river called Matanza-Riachuelo in Argentina. Environmental factors such as diarrheal diseases, respiratory diseases, and cancer are significant public health problems associated with the multiple industries in the basin which are responsible for the high level of heavy metal contamination.[3] This issue is aggravated by inadequate infrastructure in the nearby informal settlements, where residents are left with few options for drinking water.[4]

To address this problem, a user-friendly, low energy demanding and low cost treatment technology shall be developed for households, schools or other small-scale application at Instituto Technologico de Buenos Aires (ITBA), Argentina.

Nowadays, various methods have been proposed and investigated for efficient heavy metal removal from waters, including amongst others chemical precipitation, ion exchange, adsorption, membrane filtration and electrochemical technologies.[5–9] Adsorption offers flexibility in design and operation and, in many cases it will generate high-quality treated effluent with low-costs. Further there is no need for electric power or technically skilled operators which makes it attractive for the intended application.

One promising approach is an iron oxide named hematite whose affinity of heavy metals makes it possible to reduce their concentration by an adsorption process.[10] Originally developed to filter arsenic, hematite derived by Ferroxane is investigated of its ability to adsorb heavy metals, respectively chromium (trivalent and hexavalent), lead and nickel.

In the fabrication process, lepidocrocite's (iron oxyhydroxide γ-FeOOH) particle size is significantly reduced by reaction with acetic acid and then sintered to form hematite.[11] The

main advantage of hematite lies in its economics: its synthesizing costs are low compared to other treatment methods. In addition, former works have shown that there are ways to implement the hematite into an economic and user-friendly system.[12, 13]

The objectives of this research are to (i) synthesize and characterize the iron oxide particles which are used for the experiments, (ii) obtain the adsorption kinetics and isotherms (for Cr(III), Cr(VI), Ni(II) and Pb(II)) and investigate the effects of pH and ionic strength variation and finally (iii) present different possibilities to integrate the material in a process.

2 Acknowledgement

I wish to thank Professor Matthias Wessling for supervision of this work and giving me the unique opportunity to participate in this project. I would like to thank Liliana Bertini and Maria Marta Fidalgo from ITBA, Argentina and University of Missouri, USA for supervision and useful remarks.
Further I would like to thank the Ernest-Solvay-Foundation for financial support.
Last but not least, I would like to thank my colleagues at the laboratory, my parents and my brother, Diego for his patience in Spanish and Paul for his improvements and valuable comments.

3 Theory

3.1 Contamination of water by heavy metals

3.1.1 Health problems and limit values

Chromium

While chromium metal or trivalent chromium is not very toxic, hexavalent chromium Cr(VI) is carcinogenic and moderately toxic. Cr(VI) is corrosive to skin and causes denaturation and precipitation of tissue proteins.[14]
That fact makes it a special element in order of treatment and regulation because the other two considered elements are based on total concentration meanwhile chromium has to be differentiated by the oxidation state. However many concentration limits only consider the total concentration. This makes it very difficult to determine the exact toxicity of chromium.

Chromium enters natural waters by weathering of chromium-containing rocks, direct discharge from industrial operations, wet and dry deposition, and leaching from soils.
Most of the sources of Cr(VI) are from industrial activities like metal plating, dyes, paint pigments or leather tanning.[15]
In general, surface water contain between 1 and 10 μg/L but can exceed this value depending on industrial activity.[16]
The provisional guideline value of the World Health Organization recommends not to exceed a total chromium concentration of 50 μg/L for drinking water and 100 μg/L for freshwater aquatic life.[17, 18]
Argentinian law has a concentration limit of 50 μg/L as well for drinking water and for the effluents there is a concentration limit of 2 mg/L for Cr(III) and 0.2 mg/L for Cr(VI).[19]

Lead

Lead has numerous applications as metal, alloys and compounds. The major applications are as materials for construction of pipe lines, plumbing fixtures, wires, ammunition and in storage batteries.[14]

At high levels of human exposure there is damage to almost all organs and organ systems, most importantly the central nervous system, kidneys and blood, resulting in death at excessive levels. At low levels, haeme synthesis and other biochemical processes are affected.[20]

Concentrations in drinking-water are generally below 5 μg/L, although much higher concentrations (above 100 μg/L) have been measured where lead fittings are present. The primary source of lead is from service connections and plumbing in buildings.

The provisional guideline value of the World Health Organization recommends not to exceed a lead concentration of 10 μg/L for drinking water.[17]
Argentinian law has a concentration limit of 10 μg/L as well for drinking water and for the effluents there is a concentration limit of 0.5 mg/L.[19]

Nickel

The most important applications of nickel involve its use in numerous alloys such as construction equipment, reaction vessels, plumbing parts, missile and aerospace components. In catalysis nickel plays an important role as well, for example in catalytic hydrogenation or dehydrogenation.[14]

Skin contact can cause dermatitis and a type of chronic eczema, known as ”nickel itch”, caused by hypersensitivity reactions of nickel on the skin.
Although oral toxicity of the metal is very low, ingestion may cause hyperglycemia and depression of the central nervous system. Nickel and certain of its compounds are listed by IARC under Group 2B carcinogens as ”possibly carcinogenic to human” (International Agency for Research on Cancer, 1990, IARC Monograph, Vol. 49: Geneva). [21]

Concentration in drinking-water is normally less than 20 μg/L, although nickel released from

taps and fittings may contribute up to 1 mg/L. In special cases of release from natural or industrial nickel deposits in the ground, concentrations in drinking-water may be higher. The World Health Organization guideline value for drinking water is 70 μg/L. [17] No concentration limit is given by Argentinian law for Nickel.

3.2 Chemical background

3.2.1 Iron oxides

Iron oxides are compounds which are present in almost all of the different compartments of the global system: atmosphere, pedosphere, biosphere, hydrosphere and lithosphere and interact among those.
Many different scientific disciplines (see figure 3.1) have interest in these iron oxides which led to a interdisciplinary research.

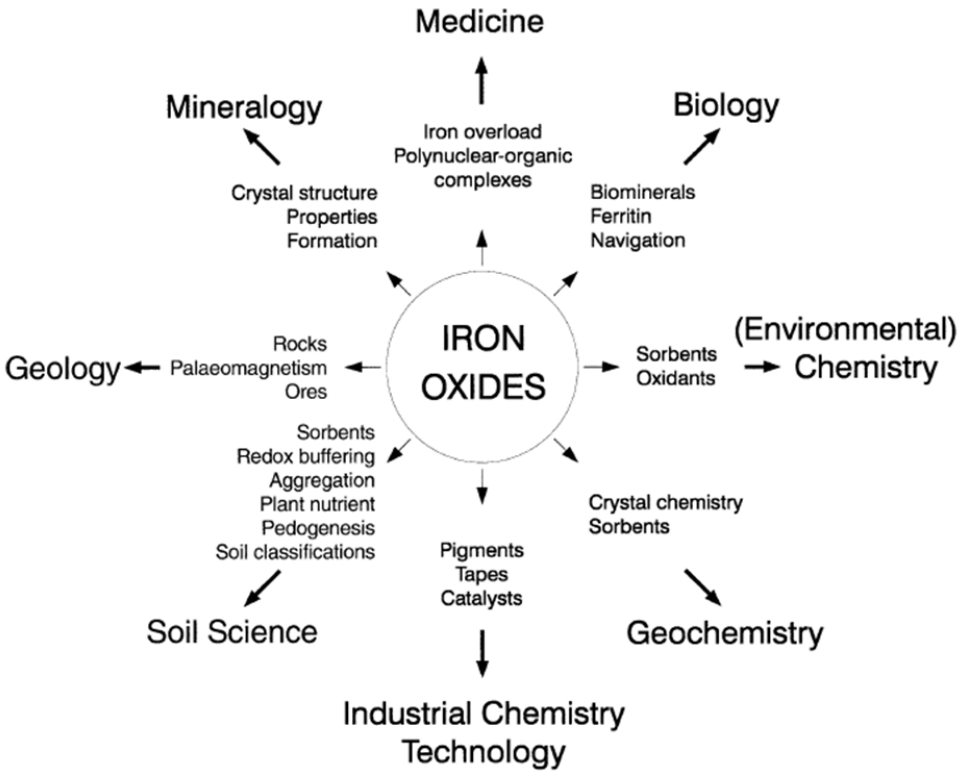

Figure 3.1: The multidisciplinary nature of iron oxide research [10]

There are 16 iron oxides which are divided into either oxides, hydroxides or oxide-hydroxides. In this work two compounds are of further interest: lepidocrocite (hydroxide) and hematite

(oxide).

In general iron oxides contain Fe together with O and/or OH and in most compounds iron is in the trivalent state.

Lepidocrocite

Lepidocrocite is one of the five oxide hydroxides called γ-FeOOH and the building unit common to all of them is the $FeO_3(OH)_3$ octahedron.

$\gamma - FeOOH$ is a layered compound with an orthorhombic cell. The structure consists of arrays of ccp (cubic close packing) anions (O^{2-}/OH^-) stacked along the direction with Fe(III) ions occupying the octahedral interstices (see figure 3.2 a-c).

Lepidocrocite is made up of double chains of $Fe(O, OH)_6$ octahedra running parallel to the c-axis. The double chains share edges with adjacent double chains forming corrugated sheets of octahedra which are held together only by hydrogen bonds (see figure 3.2 d).

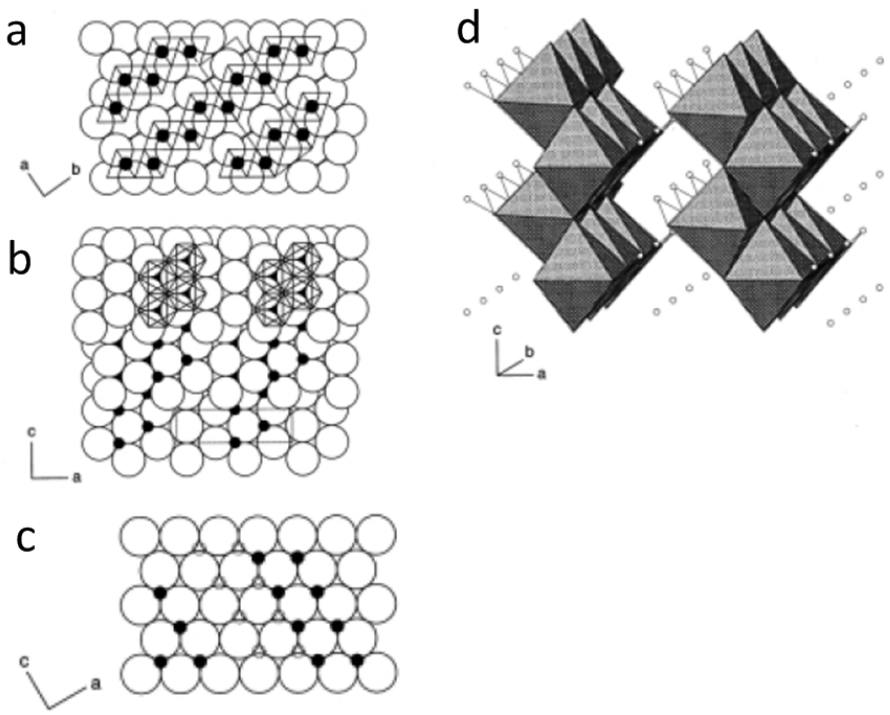

Figure 3.2: Structure of Lepidocrocite;a) Cubic close packed anion arrangement and distribution of cations over the octahedral interstices. Projection on (001). Octahedral arrangement and unit cell outlined. b) Projection on anion close packing (010). Octahedral arrangement and unit cell outlined. c) Projection on anion close packing (001). Dashed circles represent Fe in the next lower layer. d) Arrangement of octahedral double chains in corrugated layers. H-bonds between layers also shown.[10]

Hematite

Hematite is an iron oxide with an hexagonal crystallographic system. The structure of hematite consists of hcp (hexagonal close packing) arrays of oxygen ions stacked along the [001] direction, i.e. planes of anions are parallel to the (001) plane (see figure 3.3 a).
By filling two sites with Fe(III) ions and one vacant site in between in the (001) plane, two thirds of the sites are filled and thereby forming sixfold rings (see figure 3.3 b).
The arrangement of cations forms pairs of $Fe(O)_6$ octahedra which share edges with three neighboring octahedra in the same plane and one face with an octahedron in an adjacent plane (see figure 3.3 c).
Structurally hematite shares similiarities with other iron oxides, namely magnetite and goethite so growth of goethite or magnetite on hematite may occur.

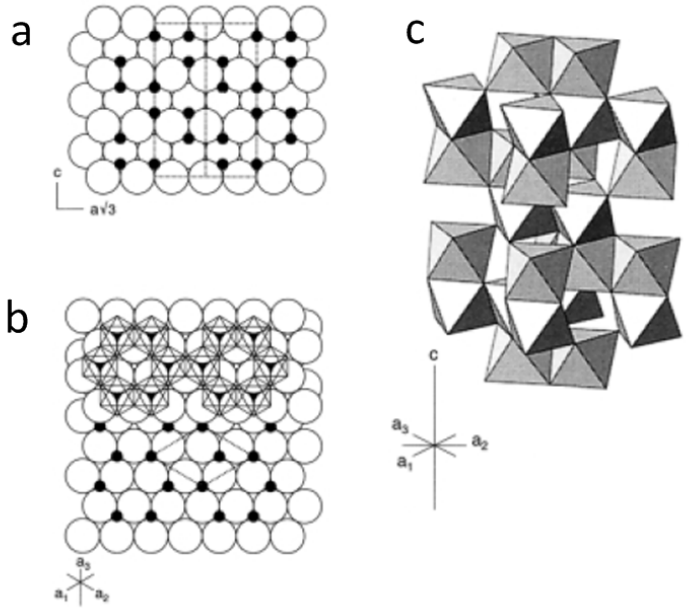

Figure 3.3: Structure of hematite; a) Hexagonal close packing of oxygens with cations distibuted in the octahedral interstices. Unit cell outlined. b) View down the c-axis shwoing the distribution of Fe ions over a given oxygen layer and the hexagonal arrangement of octahedra. Unit cell outlined. c) Arrangement of octahedra.[10]

3.2.2 Heavy metals

Chromium

Chromium is categorized as an transition metal and is widely distributed in the earth's crust. Soils and rocks may contain small amounts of chromium, almost always in the trivalent state.[22]

In natural waters chromium exists in its two stable oxidation states, Cr(III) and Cr(VI). The presence and ratio between these two forms depend on various processes, which include chemical and photochemical redox transformation, precipitation/dissolution and adsorption/desorption reactions. Under anoxic or suboxic conditions, trivalent chromium should be the only form. In oxygenated aqueous solutions, Cr^{+3} is predicted by thermodynamic calculations as the stable species at pH 4−6, whereas at pH 5−7 the ${CrO_4}^{2-}$ ions should predominate. At intermediate pH values, the Cr(III)/Cr(VI) ratio is dependent on O_2 concentration. In oxygenated surface waters, not only pH and O_2 concentration but also the

nature and concentration of reducers, oxidation mediators and complexing agents play an important role.[23]

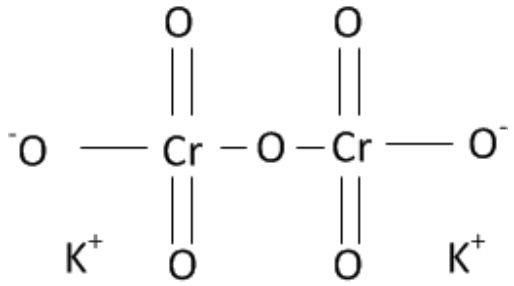

Figure 3.4: Structural formula of potassium dichromate

Two chromium compounds were used in this work, chromium(III)chloride (see figure 3.5) and potassium dichromate (see figure 3.4). In chromium(III)chloride the chromium has an oxidation state of +3 and in potassium dichromate of +6.[24]

The chromium(III)chloride used was a hexahydrate ($Cl_3Cr(6{\cdot}H_2O)$ because chromium(III)chloride is hardly soluble in water in contrary to the hexahyrate (585 g/L at 20°). The color of the solid hexahydrate is dark green and the dilute aqueous solution is violet in color. [14].

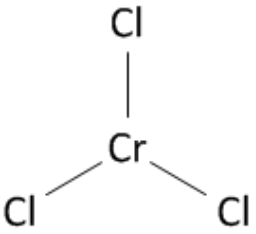

Figure 3.5: Structural formula of chromium(III)chloride

The main ions of Cr(III) in water under conditions like room temperature and trace concentrations are as follows:

$$Cr(OH)_3 + 3H^+ \rightleftharpoons Cr^{3+} + 3H_2O \tag{3.1}$$

$$Cr(OH)_3 + 2H^+ \rightleftharpoons CrOH^{2+} + 2H_2O \tag{3.2}$$

$$Cr(OH)_3 + H^+ \rightleftharpoons Cr(OH)_2{}^+ + H_2O \tag{3.3}$$

$$Cr(OH)_3 + H_2O \rightleftharpoons Cr(OH)_4{}^- + H^+ \tag{3.4}$$

Using these reactions and thermodynamic information, the Cr(III) ion distribution depending on the pH can be calculated (see figure 3.6).

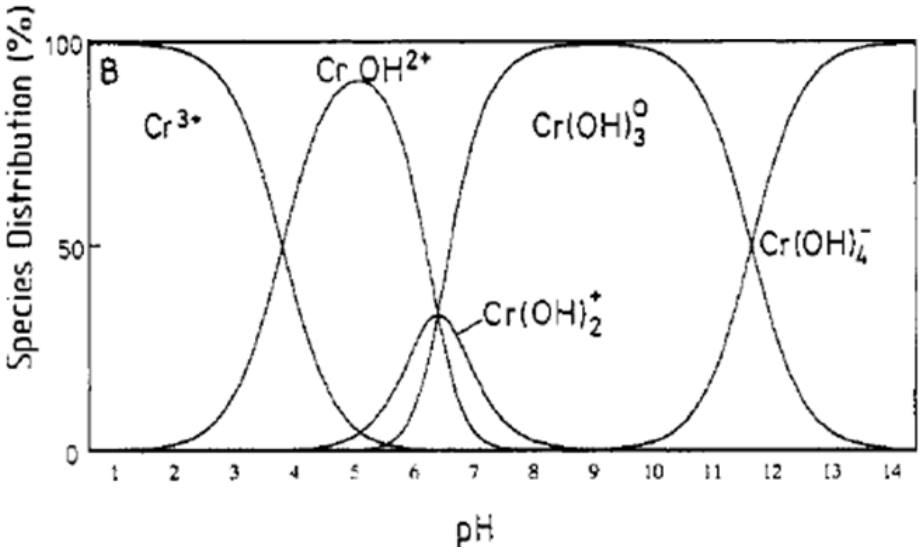

Figure 3.6: Calculated distribution of inorganic chromium(III) species as a function of pH (solution in equilibrium with $Cr(OH)_3$ precipitate) [25]

The potassium dichromate is soluble in water (49 g/L at 0°) and deionizes as follows

$$K_2Cr_2O_7 \longrightarrow 2\ K^+ + Cr_2O_7{}^{2-} \tag{3.5}$$

$$Cr_2O_7{}^{2-} + H_2O \rightleftharpoons 2\ CrO_4{}^{2-} + 2\ H^+ \tag{3.6}$$

At low pH between 2 and 6 there are also $HCrO_4{}^-$ ions present and at pH>7 the $CrO_4{}^{2-}$ is dominant. The $HCrO_4{}^-$ ions form an equilibrium reaction with the $Cr_2O_7^{2-}$ ions shown in equation 3.7. [23]
Further the $HCrO_4{}^-$ is able to convert into $CrO_4{}^{2-}$ shown in equation 3.8.

$$2\ HCrO_4^- \rightleftharpoons H_2O + Cr_2O_7^{2-} \tag{3.7}$$

$$HCrO_4^- \rightleftharpoons H^+ + CrO_4^{2-} \tag{3.8}$$

Using these reactions and thermodynamic information, the Cr(VI) ion distribution depending on the pH can be calculated (see figure 3.7).

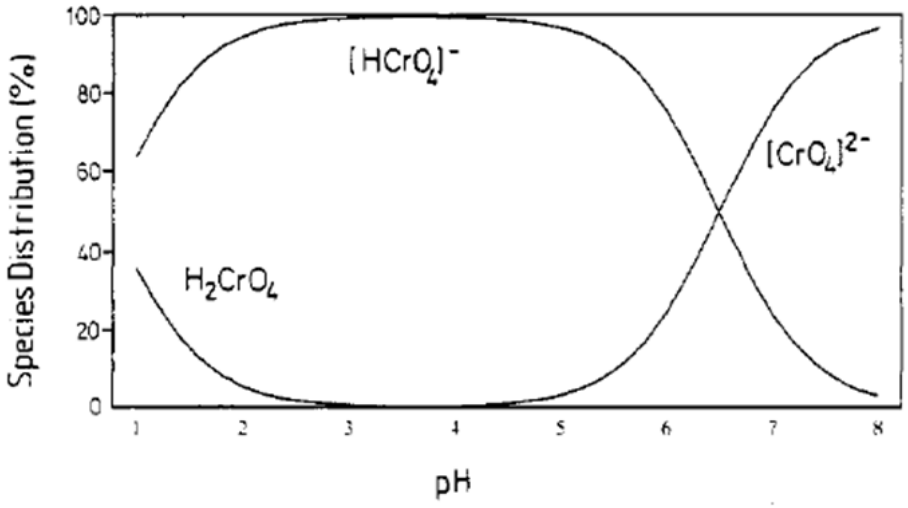

Figure 3.7: Calculated distribution of inorganic chromium(IV) species as a function of pH (10^-6 mol/L total chromium concentration) [25]

Lead

Lead is one of the oldest metals known to civilization.
It forms compounds in +2 and +4 valence states. The divalent is more common. Inorganic lead(IV) compounds are typically strong oxidants or exist only in highly acidic solutions.

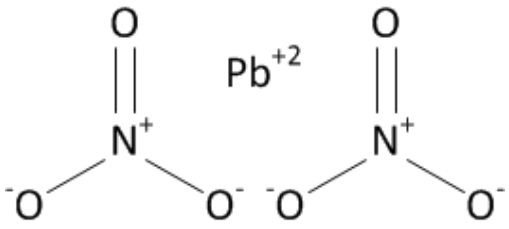

Figure 3.8: Structural formula of lead(II)nitrate

The lead compound used in this work is lead(II)nitrate (see figure 3.8) which is soluble in water (520 g/L at 20°) and has a state of oxidation of +2.[14]
Dissolved in water, it gives a clear, colorless solution and deionizes as follows [26]

$$Pb(NO_3)_2 \longrightarrow Pb^{2+} + 2NO_3{}^- \tag{3.9}$$

In figure 3.9 the distribution of lead in an aqueous solution is shown as a function of pH. Pb undergoes hydrolysis at low pH values. Above pH 9, the formation of $Pb(OH)_2$ is important, while $Pb(OH)^+$ is predominant between pH 6 and 10. [27]

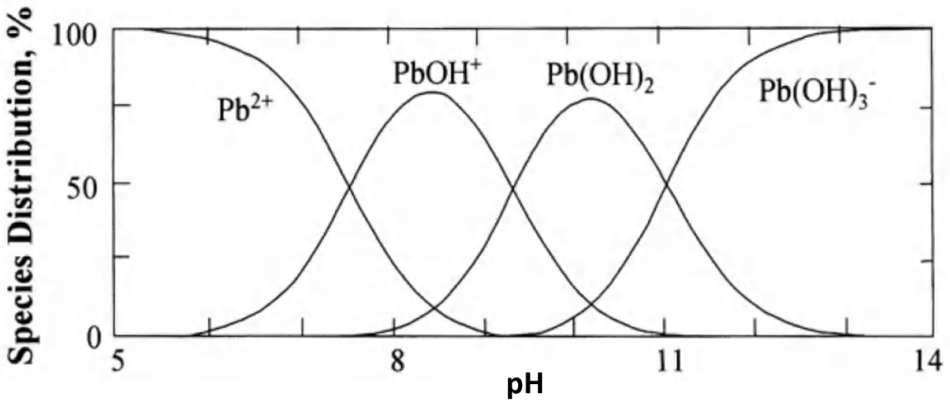

Figure 3.9: Calculated aqueous chemical speciation of lead as a function of pH [27]

Nickel

Nickel is a metallic element that is naturally present in the earth's crust.
The most common oxidation state is +2, but oxidation states of +1, +3, or +4 may also exist.[14]
The divalent state is also the predominate form of nickel in aquatic sources. [28]
The existence of other nickel compounds depends on the pH and the organic or inorganic binding-partners.
The compound used in this work is nickel(II)nitrate (see figure 3.10) which occurs as hexahydrate at ordinary temperatures. It is very soluble in water (942 g/L at 20°) and gives a green solution containing $Ni(H_2O_6)^{2+}$.[29]

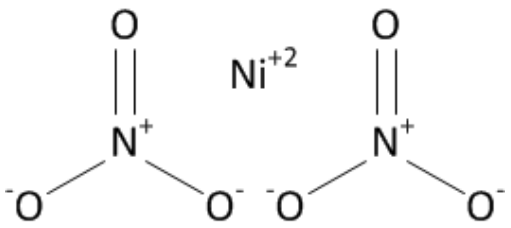

Figure 3.10: Structural formula of nickel(II)nitrate

3.2.3 Adsorption

Adsorption is a process in which atoms, molecules or ions from a gas, liquid or a dissolved solid adhere to a surface which occurs whenever they are exposed to each other. So adsorption is universally understood to mean the enrichment of one or more of the components in the region between two bulk phases (i.e. the interfacial layer).[30]
In this work the focus lies on dissolved metal ions in water which enrich on an iron oxide, respectively hematite. To get an overview and to understand adsorption better, table 3.1 explains the most important terms briefly.

Table 3.1: Definition of adsorption terms [30]

Term	**Definition**
Adsorption	Enrichment of one or more components in an interfacial layer
Adsorbate	Substance in the adsorbed state
Adsorptive	Adsorbable substance in the fluid phase
Adsorbent	Solid material on which adsorption occurs
Chemisorption	Adsorption involving chemical bonding
Physisorption	Adsorption without chemical bonding
Monolayer	capacity either Chemisorbed amount required to occupy all surface sites or Physisorbed amount required to cover surface
Surface coverage	Ratio of amount of adsorbed substance to monolayer capacity

Further the International Union of Pure and Applied Chemistry (IUPAC) published a classification [31] of pore sizes in 1985 shown in table 3.2. The pore width is defined as the

diameter in case of a cylindrical pore and the distance between opposite walls in case of a slit pore.

Table 3.2: Classification of pores according to the IUPAC

	Width [nm]
Micropores	< 2
Mesopores	2 - 50
Macropores	>50

In general, there are two main objectives of studies with iron oxides regarding adsorption[10]:

- Measurement of the amount of adsorptive after adsorption to calculate the amount absorbed and further the kinetics or isotherms
- Spectroscopic investigation of the adsorption surface to understand better the chemical and physical processes at the surface

This work focuses on the first objective and therefore kinetic and equilibrium models are explained more detailed in the following section. Mathematical models can describe the different types of adsorption under certain conditions and so help to perform optimization or scale up processes.[32]

3.2.4 Adsorption Kinetics

The dynamics of adsorption give information about the time to reach equilibrium and the absorptive uptake rate. Various models have been suggested and three well-known models (Pseudo-first, pseudo-second order and Elovich) were selected to fit the kinetic experiment results.

Pseudo-first order or Lagergren kinetic model

The model, first developed by Lagergren in 1898, is based on the concentration of solution and adsorption capacity of solid.[33]

The differential equation for the model is shown in equation 3.10 with Q_e as adsorption capacity at state of equilibrium, Q_t at time t and k_1 as a constant rate:

$$\frac{dQ_t}{dt} = k_1(Q_e - Q_t) \tag{3.10}$$

After solving equation 3.10 and given a boundary condition that at $t = 0$, the concentration of the adsorbate at the surface equals 0, the model can be expressed as:

$$\ln(Q_e - Q_t) = \ln(Q_e) - k_1 t \tag{3.11}$$

With this linearization, k_1 can be determined from the slope by plotting $\ln(Q_e - Q_t)$ vs. t. The difference to a true first-order model is that Q_e normally should be calculated from the intersection with the vertical axis at $t = 0$ but in this case, it can be used an adjustable parameter.[32, 34]

Pseudo-second-order kinetic model

The differential equation for this model is shown in equation 3.12 with k_2 as the rate constant of pseudo-second-order adsorption[32, 35]:

$$\frac{dQ_t}{dt} = k_2(Q_e - Q_t)^2 \tag{3.12}$$

Solving the equation with the same boundary condition as equation 3.10 gives equation 3.13:

$$\frac{1}{Q_e - Q_t} = \frac{1}{Q_e} + k_2 t \tag{3.13}$$

and linearized to obtain k_2 from the plot of $\frac{t}{Q_t}$ vs t is Eq. 3.14

$$\frac{t}{Q_t} = \frac{1}{k_2 {Q_e}^2} + \frac{t}{Q_e} \tag{3.14}$$

The Elovich kinetic model

The Elovich kinetic model was originally formulated to describe oxidation processes[36] and later Elovich, Roginski and Zeldovich used it to develop the kinetic model for adsorption. The model is shown in equation 3.15

$$\frac{dQ_t}{dt} = \alpha e^{\beta Q_t} \tag{3.15}$$

where α is the initial adsorption rate, β as the desorption constant and Q_t as the amount adsorbed at time t.
Solving this differential equation with the boundary conditions $Q_t = 0$ at $t = 0$ and $Q_t = Q_t$ at $t = t$ gives equation 3.16.[37]

$$Q_t = \frac{1}{\beta}\ln(\alpha\beta) + \frac{1}{\beta}\ln(t + \frac{1}{\alpha\beta}) \tag{3.16}$$

With the assumption of $\alpha\beta \gg \frac{1}{t}$, the equation can be linearized, shown in equation 3.17. [38, 39] .

$$Q_t = \frac{1}{\beta}\ln(\alpha\beta) + \frac{1}{\beta}\ln(t) \tag{3.17}$$

With a plot of Q_t vs $\ln(t)$ the constants can be obtained from the slope and the interception.

3.2.5 Adsorption Isotherms

Adsorption isotherms relate the data of material adsorbed to the adsorbent to the equilibrium concentration of the solution at a constant temperature.[40]
Although they might help making limited predictions about the behaviour of the adsorption, they give no information about the mechanism of adsorption nor the existing complexes at the surface.[10]

Classification of isotherms

A lot of isotherms are recorded experimentally on gas-solid systems and most of them can be grouped into six classes in the IUPAC classification which are shown in figure 3.11.

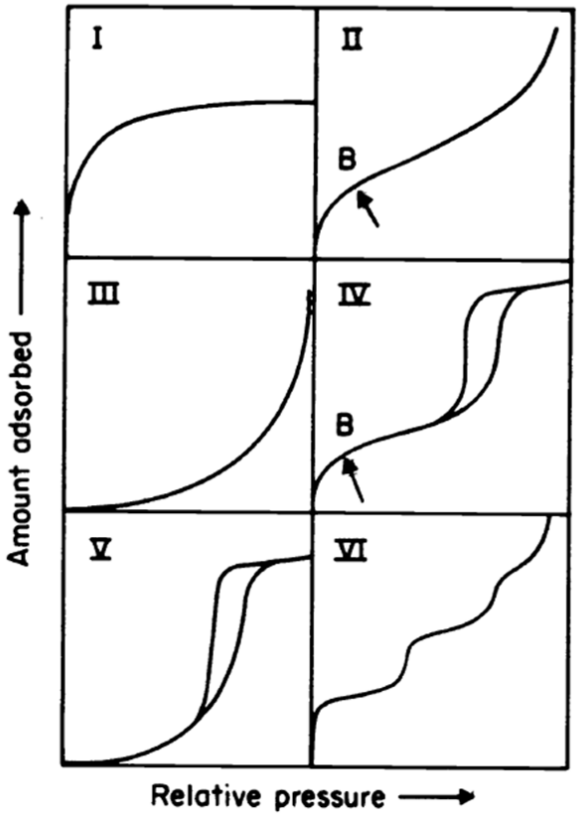

Figure 3.11: IUPAC classification of six main sorption isotherms [41]

- Type I is a reversible concave isotherm which approaches a limit when the relative pressure converges 1. Mostly microporous solids with a relatively small external surface like activated carbons or molecular sieve zeolites are type I where the maximum uptake is controlled by the accessible micropore volume and adsorption is limited to, at most, only a few molecular layers.

- Type II reversible sorption isotherms are typically obtained by non-porous and macroporous solids where unrestricted monolayer-multilayer adsorption can occur. The inflection point (Point B) indicates where the monolayer coverage is complete and multilayer adsorption begins.

- Type III reversible sorption isotherms are very uncommon and are convex to the rela-

tive pressure axis over the entire range.

- Type IV isotherms have a characteristic hysteresis loop which is because of capillary condensation taking place in mesopores. The path of the type IV isotherm is similar to the type II isotherm which reasons in the same monolayer-multilayer characteristics.
- Type V is not common and is related to the type III isotherm.
- Type VI isotherms are a stepwise multilayer adsorption in which every step represents a monolayer capacity. [30, 41, 42]

For the interpretation of the hysteresis loops, there is a classification of four different types of hysteresis loops depending on the type of pores of the adsorbent which are shown in figure 3.12.[31]

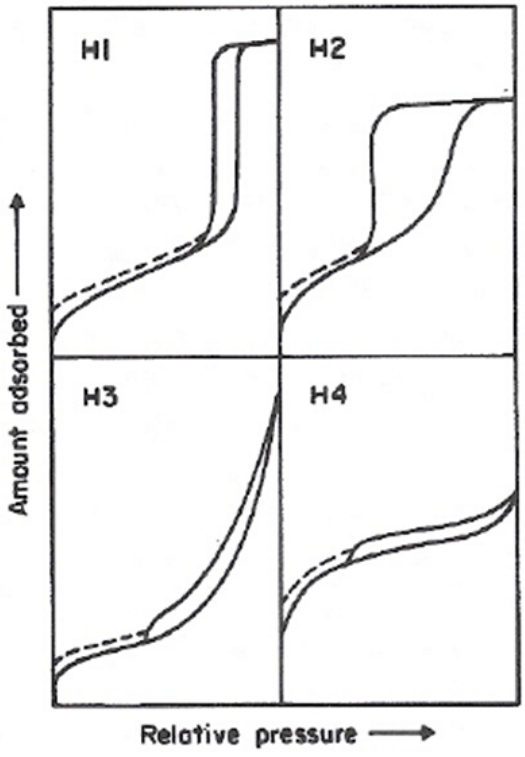

Figure 3.12: Types of hysteresis loops [31]

- H1 well defined cylindrical pore channels
- H2 disordered pores (pore blocking, percolation phenomena)
- H3 non-rigid aggregates of plate-like particles (slit-shaped pores)
- H4 narrow slit pores including pores in the micropore region

This work focuses on a fluid-solid system but nevertheless these classifications are important for the determination of the surface and porosity of the hematite used by the BET-method described in section 4.3.1.
The following equations are different types of isotherm models to describe the behavior of the adsorption process. The easiest one would be a linearization which only appears to be valid at a low surface coverage and low relative pressure and often is referred to as the Henry's Law region.[41]

Langmuir isotherm equation

Langmuir originally derived this equation in 1918 from studies[43] on gas adsorption to activated carbon.[32]
The model assumes a homogeneous surface and only a monolayer uptake so adsorption can only occur at a finite number of locations. Furthermore there is no transmigration of the adsorbate, constant enthalpy and sorption activation energy.[44]
The Langmuir equation is shown in equation 3.18 with Q_e as the adsorbed metal concentration, Q_{max} as the maximum specific uptake, C_{eq} as the metal residual concentration in the solution and b as the ratio of adsorption and desorption rates.

$$Q_e = \frac{Q_{max} b C_{eq}}{1 + b C_{eq}} \tag{3.18}$$

This equation can be linearize which enables to calculate the b and the Q_{max} with experimental data from isotherm experiments (shown in equation 3.19). For a further discussion and more possibilities to linearize, also see section 5.3.

$$\frac{1}{Q_e} = \frac{1}{Q_{max}} + \frac{1}{Q_{max} b} \frac{1}{C_{eq}} \tag{3.19}$$

Freundlich isotherm equation

The Freundlich isotherm, first introduced in 1906, can be applied to multilayer adsorption onto heterogeneous surfaces with non-uniform distribution of adsorption heat.[45]
It has been derived by assuming an exponentially decaying site energy distribution and is

often criticized for the lack of a fundamental thermodynamic basis since it does not reproduce Henry's Law at low concentration.[46]
The isotherm is expressed by equation 3.20 with Q_e as the amount adsorbed, n as the adsorption intensity, K_f as the Freundlich constant and C_{eq} is the residual concentration of the metal in the solution.[44]

$$Q_e = K_f C_{eq}^{\frac{1}{n}} \tag{3.20}$$

Linearly, the equation is expressed as equation 3.21:

$$\log(Q_e) = \log(K_f) + \frac{1}{n}\log(C_{eq}) \tag{3.21}$$

Temkin isotherm equation

The Temkin isotherm [47] is derived by the assumption of a uniform distribution of binding energy and takes into account the adsorbent-adsorbate interactions. Further it assumes that the heat of adsorption rather decreases linearly than logarithmic with coverage.[44]
Equation 3.22 shows the nonlinear form and equation 3.23 expresses the linear form.

$$Q_e = \frac{RT}{b_T}\ln(A_T C_{eq}) \tag{3.22}$$

$$Q_e = \frac{RT}{b_T}\ln(A_T) + \frac{RT}{b_T}\ln(C_{eq}) \tag{3.23}$$

R is the universal gas constant, T the absolute temperature, the constant b_T is related to the heat of adsorption, A_T is the equilibrium binding constant corresponding to the maximum binding energy.[32]

3.2.6 Zeta potential

A particle in a liquid develops a nett charge at the particle surface which affects the distribution of ions in the surrounding interfacial region. This results in an increased concentration of counter ions (opposite charge of the particle surface) close to the surface, thus an electric double layer exists around each particle (see figure 3.13).

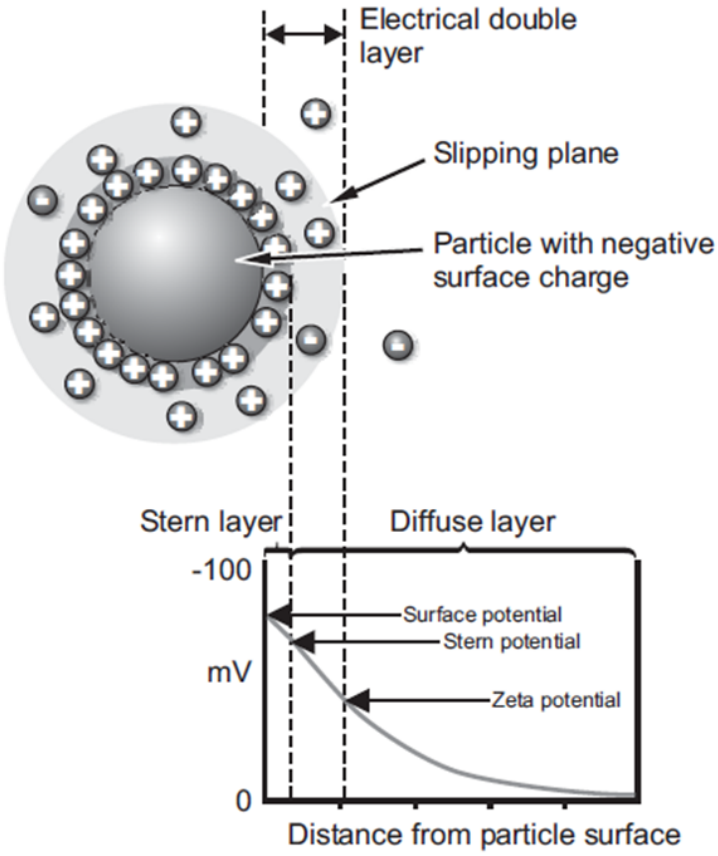

Figure 3.13: Particle surrounded by ions and the different potentials [48]

The liquid layer around the particle can be divided into two parts; an inner region called the Stern layer, where the ions are strongly bound and an outer, diffuse region, where they are less firmly attached.

If a particle moves in the fluid, ions within the boundary move with it, but ions outside the boundary do not. This boundary is called the surface of hydrodynamic shear or slipping plane. The potential that exists at that boundary is called zeta potential.

The magnitude of the zeta potential is an indicator of the potential stability of the colloidal system. In a suspension with a large positive or negative zeta potential, the particles will tend to repel each other and have no tendency to aggregate. However, if the zeta potential

is low there is no force preventing the particles from aggregating. General dividing line between stable and unstable suspensions are either $+30mV$ or $-30mV$. In many cases the most important influence on the zeta potential is the pH besides other factors such as temperature or size of the particles.
The point where the plot of zeta potential vs pH passes through zero is called the Isoelectrical point. It is normally the point where the suspension is the least stable. [48]
In this work metal ions are observed being adsorbed on a bulk solid. This process is strongly influenced by the surface charge of the colloidal substrate (in this case hematite) for which the zeta potential is used as a surrogate. Vice versa the metals influence the surface charge of the colloidal substrate.[49]

3.3 Analytical background

3.3.1 Atomic absorption spectroscopy

Atomic spectroscopy is the oldest instrumental elemental analysis principle, which originated by the work of Bunsen and Kirchhoff in the mid-19th century.[50]
In the 1950's, the use of flames as atom reservoirs for atomic absorption spectrometry was transformed into an analytical methodology, as a result of the efforts of Walsh[51] which then became a standard tool of the routine analytical laboratory.[52]

The principle of atomic absorption is based on the fact that atoms of elements absorb light at a certain wavelength. Generally, the selectivity of this process is very high because each wavelength only corresponds to one element and these absorption lines are very thin. This absorption can be measured and described quantitatively with a comparative method.
Therefore the sample has to be atomized. This can be done with different types of atomizers but this work only used the flame atomizer because of its mg/L measure range. It uses an air-acetylene flame with a temperature of about 2300°C or a nitrous oxide-acetylene-flame with a temperature of about 2700°C to vaporize the sample depending on the element measured.[53]
The optical path passes through the flame with the atomized sample and is partly absorbed.

Behind the flame the beam enters a monochromator and is finally detected. This detection is processed and shown on the connected device (see figure 3.14).

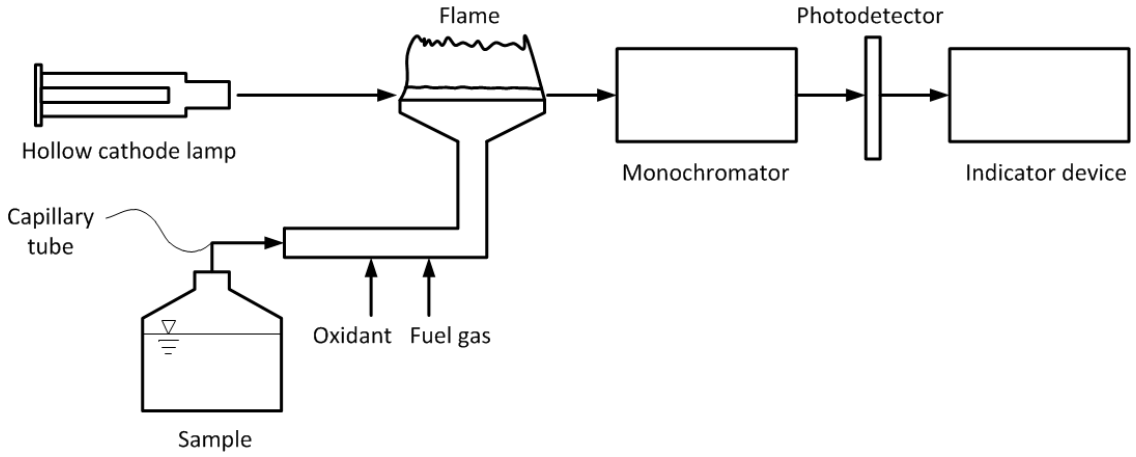

Figure 3.14: Basic components of an atomic absorption spectroscope

The difference between the intensities of the detected light can be used to correlate with the concentration in the sample by calibrating with standardized solutions. The relationship between the absorbance and the concentration of the absorbing atoms in an atom reservoir is given by the Lambert-Beer law (see equation 3.24).

$$A \;=\; \log\left(\frac{I_0}{I}\right) \;=\; k \cdot c \cdot l \tag{3.24}$$

where

- A is the absorbance
- I_0 is the intensity of the incident radiation
- I is the intensity of the exiting radiation
- l is the length of the atom reservoir
- c is the concentration of the sample

However, the Lambert-Beer law is only valid in a restricted concentration range (for most solutions less than 0.01 mol/L). The reason for this is the fact that not all radiation reaching the detector has been absorbed to the same extend by the sample atoms.[54]

3.3.2 Nitrogen adsorption measurements

Being able to calculate the surface area depends on the ability to predict the number of molecules required to cover the surface of the measured sample. With this information, the surface area can be calculated by multiplying the number of molecules for a single layer with effective crossectional area of the adsorbed molecule.[42]
These calculations depend on different assumptions which depend on the model used. The BET theory was developed by Brunauer, Emmett and Teller in 1938 and is the most commonly used model to predict the specific surface area by measuring the adsorption isotherms (see section 3.2.3).
The pore size calculations are based on the BJH (Barrett, Joyner and Halenda) method which uses the Kelvin equation to correlate relative pressure of nitrogen in equlibrium to the size of the pore (where capillary condensation takes place).

BET theory (Brunauer, Emmmett and Teller) [55]

The BET model is an extension of Langmuir's kinetic theory and enables a determination of the number of molecules required to form a monolayer on the surface of an adsorbent without actually having an existing monolayer.
The model assumes that the uppermost molecules of the stacks formed by the adsorbate are in dynamic equlibrium with the vapor. So if there is only one layer, that molecule is in dynamic equilibrium with vapor and where there is more than one layer, the upper layer is in state of equilibrium. This dynamic equilibrium means that the location may vary of the covered surface sites (by one or more layers) but the number of molecules in each layer remain constant.
The BET model can be described by the following equation

$$\frac{1}{W_a\,(p/p_0 - 1)} = \frac{1}{W_m C} + \frac{C-1}{W_m C} \cdot \left(\frac{p}{p_0}\right) \tag{3.25}$$

where

- W_a is the total absorbed weight

- W_m is the weight adsorbed in a completed monolayer
- C is a constant
- p is the actual pressure
- p_0 is the saturation pressure of the gas at a certain temperature

By plotting equation 3.25 against relative pressure $\frac{p}{p_0}$ in a relative pressure range, a straight line is obtained with a slope of $\frac{C-1}{W_m C}$ and an interception at $\frac{1}{W_m C}$ to determine the needed constant and the weight of the monolayer.

The total surface area can be calculated from equation:

$$S_t = N_m A_x = \frac{W_m \overline{N} A_x}{\overline{M}} \tag{3.26}$$

where

- S_t is the total surface area
- N_m is the number of adsorbate molecules in a completed monolayer
- A_x is the cross-sectional adsorbate area
- $\overline{M}$ is the adsorbate molecular weight
- $\overline{N}$ is the Avogadro number

The total pore volume is determined usually at $p/p_0 = 0.95$, in this case the adsorbed amount reflects the adsorption capacity and the total specific pore volume can be calculated:

$$V_p = \frac{W_a}{\rho_l} \tag{3.27}$$

- V_p pore volume
- W_a total absorbed amount
- ρ_l liquid density

The specific surface area and specific pore volume can be determined by dividing S_t and V_p by the sample weight, respectively.

The standard adsorptive for surface area measurements is Nitrogen, its unique properties have led to its acceptance in this role with an assigned cross-sectional area of 16.2 $Å^2$ at its boiling point of 77.35 K.

BJH theory (Barrett, Joyner and Halenda) [56]

For the pore size distribution the desorption isotherm is used which is constructed by plotting the volume desorbed per gram of sample against the relative pressure, $\frac{p}{p_0}$. The desorbed volume is used to convert to equivalent liquid volumes because it is assumed that capillary condensation occured and the pores are filled with liquid. To obtain the liquid volume, the gas volume is multiplied by 0.00156 which is the conversion from gas to liquid at STP. Further it is assumed that the pores are cylindrical.

The Kelvin equation is applied to calculate the core radius of the liquid in the capillary shown in equation 3.29.

$$RT \ln(\frac{p_s}{p_o}) = -2\gamma \frac{V_M}{R_k} \tag{3.28}$$

where

- R_k is the Kelvin radius
- γ is the adsorbate surface tension at T $[\frac{mN}{m}]$
- R is the gas constant
- T is the boiling point of nitrogen
- V_m is the molar volume of nitrogen

Substituting for the values of the constants and solving for R_k gives

$$R_k = -4.14 \log(\frac{p_s}{p_0}) \tag{3.29}$$

in Angstrom.

The actual pore radius is assumed to be addition of the core radius of the liquid and the film thickness of the liquid nitrogen. Therefore the modified Halsey equation [57] (see equation 3.30) is used to calculate the nitrogen film adsorbed on the walls of the pore at a given relative pressure.

$$t \;=\; 3.54 \left[\frac{5}{2.303 \log \frac{p_0}{p_s}} \right]^{\frac{1}{3}} \tag{3.30}$$

- t is thickness of the nitrogen film in Angstrom

The values used for the different constants are given below.

- Surface tension of nitrogen, $\gamma \;=\; 8.855 \; \frac{mN}{m}$
- Molar volume, $V_m \;=\; 34.6 \; \frac{cm^3}{mole}$
- Normal boiling point of N_2, T $\;=\;$ 77.3 K
- Ideal gas constant, R $\;=\; 8.314 \; \frac{J}{mol \; K}$

3.3.3 Dynamic light scattering

Dynamic light scattering measures the Brownian motion and relates this to the size of the particles. This is done by analyzing the intensity fluctuations of the scattered light by the particles.
A laser is used to illuminate the particles in a solution and the scattering is detected in a certain angle (see figure 3.15).

The particles are constantly moving due to the Brownian motion. Small particles move quickly and large particles move more slowly. This relationship between the size of the particle and its speed caused by the Brownian motion is defined in the Stokes-Einstein equation.
The rate of the intensity fluctuation on the detector is measured and then used to calculate the size of the particles.[48]
Dynamic light scattering is now widely used as a very convenient and nondestructive method

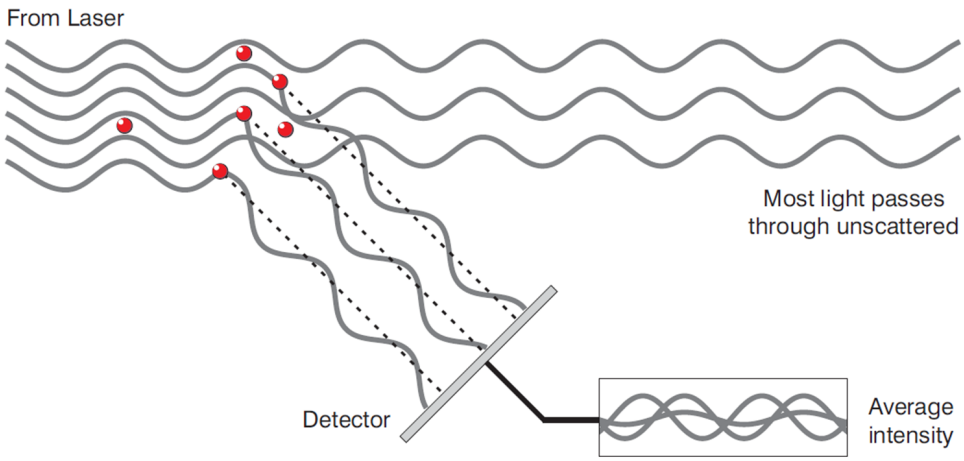

Figure 3.15: Dynamic light scattering: scattered light falling on the detector [48]

for particle sizing. The technique is suitable for the characterization of colloidal particles over a wide range of sizes from a few nanometers to several micrometers.[58]

3.3.4 Zeta potential

To measure the zeta potential, the fact is used that when a electrical field is applied across an eletrolyte, charged particles are attracted towards the electrode of opposite charge. When equilibrium is reached between the electric force and the opposing viscous force, the particles move with a constant velocity. This velocity reffered as eletrophoretic mobility depends on the following factors:

- Strength of the dieletric field or voltage gradient
- The dieletric constant of the medium
- The viscosity of the medium
- The zeta potential

Knowing these influences, the zeta potential can be obtained by the application of the Henry equation (see equation 3.31).

$$U_E = \frac{2\epsilon z f(Ka)}{3\eta} \tag{3.31}$$

where

- z is the zeta potential
- U_E is the eletrophoretic mobility
- ϵ is the dieletric constant
- η is the viscosity
- $f(Ka)$ is the Henry's function

When eletrophoretic determinations of zeta potential are made in aqueous media with moderate electrolyte concentration, $f(Ka)$ is set to 1.5 and is referred as the Smoluchowski approximation. That assumption is valid for systems with particles larger than 0.2 μm dispersed in eletrolytes containing more than $10^{-3}M$ of salt.[48].
To measure the electrophoretic velocity laser doppler velocimetry is used where the rate of fluctuation of scattered light combined with a reference beam is proportional to the speed of the particles.

4 Materials and Methods

4.1 Chemical synthesis

To obtain the adsorbent powder, a reaction took place in three steps:
lepidocrocite (section 4.1.1), ferroxane (section 4.1.2) and hematite (section 4.1.3). All chemicals used were of reagent grade. The water used for all reactions was purified by reverse osmosis.

4.1.1 Lepidocrocite

The synthesis of lepidocrocite was carried out in the laboratory by a pH controlled oxidation of ferrous chloride $FeCl_2$ (28-32% w/w) obtained from PPE Argentina S.A according to a previously published method in [10].
$FeCl_2 \cdot 4H_2O$ solution (100 mL) was mixed with a NaOH solution in a ratio $R = \frac{FeCl_2 \cdot 4H_2O}{NaOH} = 0.6$ which favors the formation of pure lepidocrocite.[10]
The mixture was kept at room temperature and stirred with about 200 rpm. To control the pH at 7, a control module was installed which used 1 M NaOH from a tank beside to regulate the pH in the reactor shown in figure 4.1. Aeration was accomplished by a commercial air pump. The reactor was stirred for about three hours and then kept overnight in the laboratory.

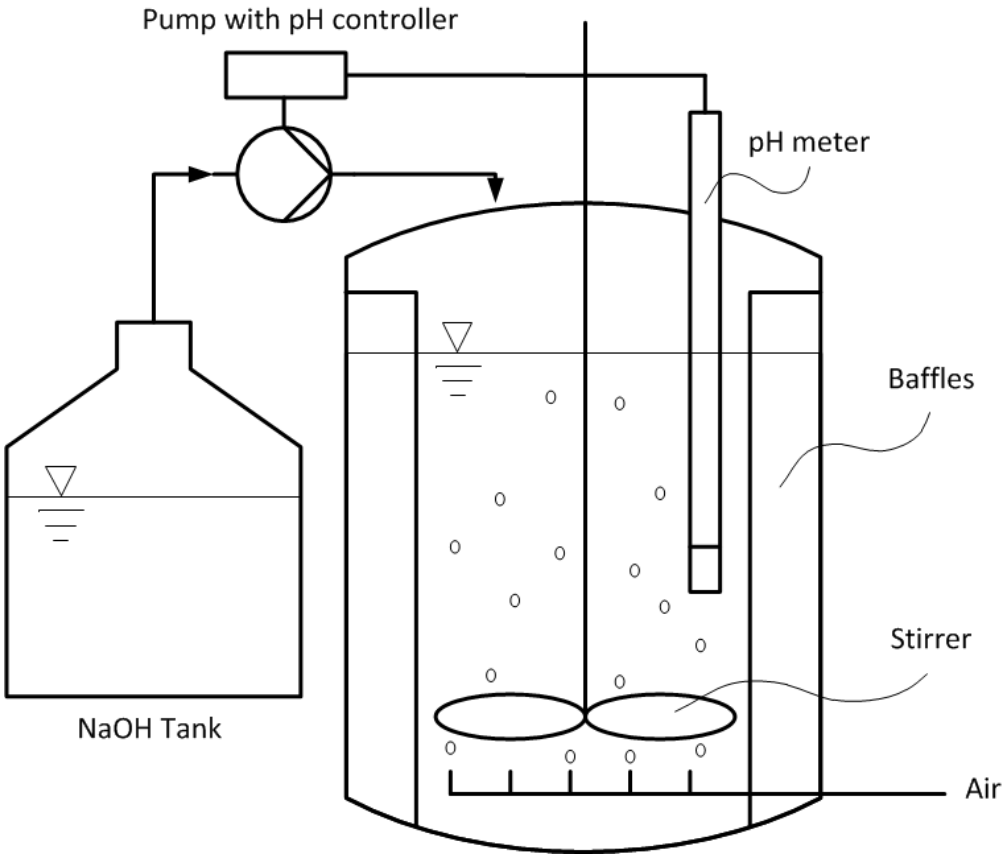

Figure 4.1: Reactor setup for lepidocrocite reaction

After the reaction took place, the product was washed and centrifuged three times before drying it in a crystallizer. It was reported and tested in the laboratory before that this reaction under these conditions leads to a compound which is composed 100% of $\gamma - FeOOH$, respectively lepidocrocite, so no further analysis was performed in this case.[11]

4.1.2 Ferroxane

10 g of dried and crushed lepidocrocite and $11.38mL = 0.1894$ mol of a 100% acetic acid solution (Anedra Argentina) were refluxed in water (250 mL) at 80°C for three hours. The reaction setup is shown in figure 4.2 and the temperature of the water was automatically controlled.

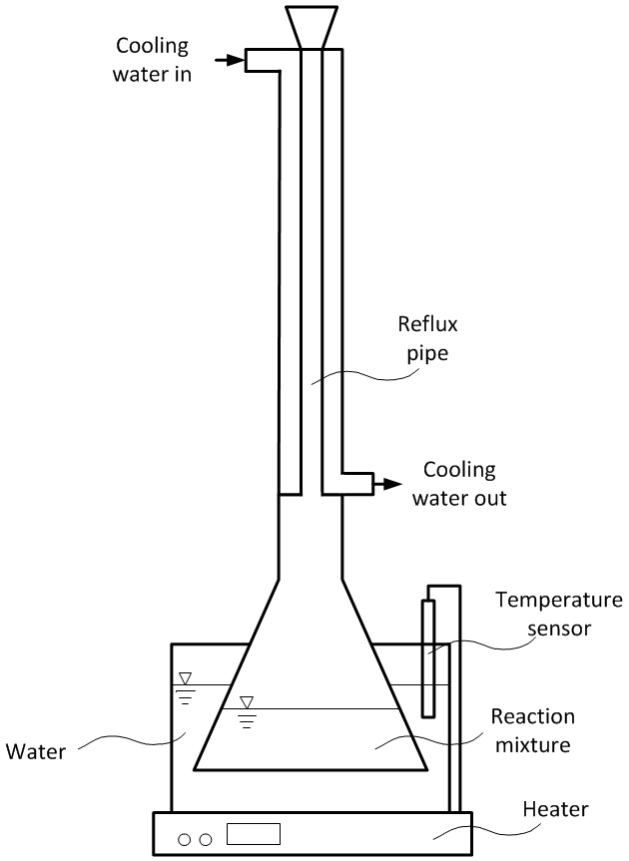

Figure 4.2: Reaction setup for Ferroxane

After the reaction, the compound is centrifuged and only the fluid part is kept and dried in a crystallizer. The solid part includes the non-reacted compounds of lepidocrocite.
The product of this reaction is carboxylate-FeOOH nanoparticles named Ferroxane-AA.[12]

4.1.3 Hematite

To obtain the final product hematite, the Ferroxane needed to be sintered. Therefore the Ferroxane flakes were crushed and put into an oven. The exact firing program is shown in figure 4.3 and was found to be the most effective in order to keep a maximum surface area of the particles by avoiding aggregation by former works at the institute. After the procedure the hematite was left until cooled down to ambient temperature.

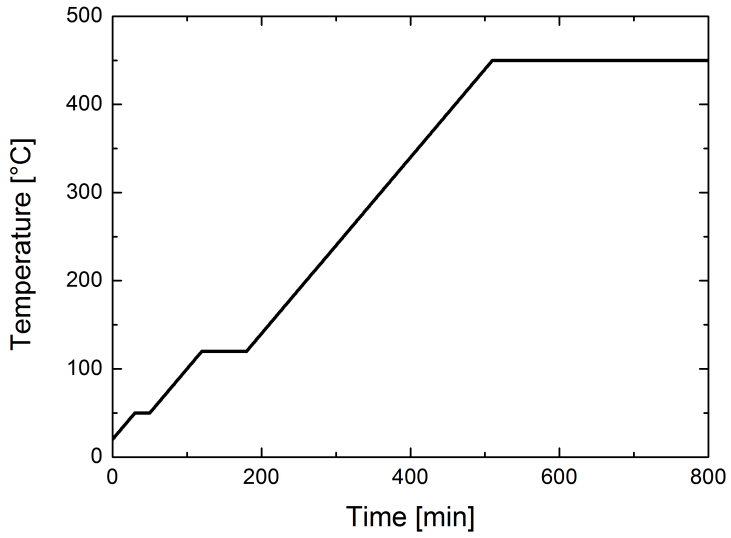

Figure 4.3: Temperature sequence for the sintering process

Following on the procedure, the hematite was analyzed.

The specific surface area was conducted by Brunauer-Emmet-Teller (BET) N_2 method and the pore size was calculated by the Barrett, Joyner and Halenda (BJH) N_2 adsorption/desorption method at 77K using the Coulter^{TM} SA 3100^{TM} analyzer (see section 4.3.1). The particle size was obtained by dynamic light scattering using a Malvern^{TM} Zetasizer Nano ZS (see section 5.1.2).

Further the crystallographic structure of the hematite was determined by an external institute with the help of Dr. Maria Marta Fidalgo at the Civil and Environmental Engineering Department, University of Missouri, USA by using X-ray diffraction chromatography (see section 5.1.3).

4.2 Experiments

4.2.1 Heavy metals

The basic setup for all experiments was a fixed concentration of each metal of 10 mg/L. The different metals were in different ionic forms: Pb and Ni were divalent, Cr was tested trivalent and hexavalent.

To have a consistent concentration in all experiments, a stock solution of 1 L was prepared with a concentration of 100 mg/L for each metal. These solutions were obtained by calculating the molar masses of each compounds used shown in table 4.1 and taking into account the molar fraction of the metal in the molecule. The following section shows exemplary this calculation for Cr(III).

The molar weight of Chromium(III)chloride is $266.5\frac{g}{mol}$ and the wanted concentration is 100 mg/L in 1 L in solution which means in mass fraction $100\frac{mg}{kg}$. The density of water at laboratory conditions is assumed to be $1000\frac{kg}{m^3}$ for small concentrations which leads to a wanted mass of 100 mg of Cr in 1 L water solution. 100 mg of Cr are $1.9232 \cdot 10^{-3}$ mol. The molar fraction of Cr in Chromium(III)chloride is $\frac{52.0}{266.5}$ which is about 0.1951. So the final amount needed is calculated by dividing 100 mg times the fraction of Cr in the compound and multiplying it with the purity of the product given by the manufacturer (for the result, see table 4.1). In case the metal appears more than one time in the compound (for example Cr(VI)), this has to be taken into account.

Table 4.1: Compounds used to prepare the metal ion solutions of 100 mg/L concentration

Metal ion	**Compound used**	**MW** $[\frac{g}{mol}]$	**Amount used for 1L [g]**	**Purity**
Cr(III)	$Cl_3Cr \cdot 6H_2O$	266.5	0.5229	98%
Cr(VI)	$K_2Cr_2O_7$	294.2	0.2858	99%
Ni(II)	$N_2NiO_6 \cdot 6H_2O$	290.8	0.4954	99.9%
Pb(II)	$Pb(NO_3)_2$	331.2	0.1605	99.5%

For the experiments which needed a metal ion concentration of 10 mg/L, a 100 mL volumetric flask was filled with stock solution, put into a 1 L volumetric flask and filled with water. So the process of weighing the metal only had to be done one time for each metal to avoid measuring small amounts of solid.

4.2.2 Kinetics of adsorption

To investigate the adsorption capacity over time, basic kinetic adsorption experiments were conducted. The experiments for all metals were observed for 72 hours and the concentration of the adsorbent in the suspension was chosen to be $1\frac{g}{L}$. Further the ionic strength was set to be 10 mM and was adjusted by using sodium nitrate ($NaNO_3$, J.T.Baker 99.3%) as a salt. This salt was also used in other kinetic studies to observe adsorption characteristics of different iron oxides.[13, 59]
The pH was fixed for each metal (see table 4.2) by using 1 M NaOH or 1 M HCL to set the pH before adding the adsorbent. To keep the pH constant over time, MES (2-(N-morpholino)ethanesulfonic acid) obtained from Sigmal Aldrich was added as a buffer with a concentration of $5\frac{mmol}{L}$. The choice of the pH was done in compliance with the experiences of former works conducted by Instituto Technologico de Buenos Aires (ITBA), Argentina as well as the figure 4.6 in which the adsorption capacities of Pb and Ni are shown. Further as an orientation, a regular pH of surface and drinking water was taken into account which is about between pH 5-7.
To prepare the solutions, stock solution, salt and buffer was added. Then it was diluted to the desired concentration and the pH was fixed. The final step was adding the hematite right before the experiment.

Table 4.2: Conditions of the kinetic adsorption experiments

Metal ion	pH	Ionic strength [mM]	Adsorbent concentration [g/L]
Cr(III)	5	10	1
Cr(VI)	5	10	1
Ni(II)	7	10	1
Pb(II)	5	10	1

In figure 4.4 the basic setup for the experiment is shown. Agitation was achieved by magnetic stirring and the erlenmeyer flasks were sealed with parafilm. The experiments were conducted at ambient temperature ($20 - 25°C$).

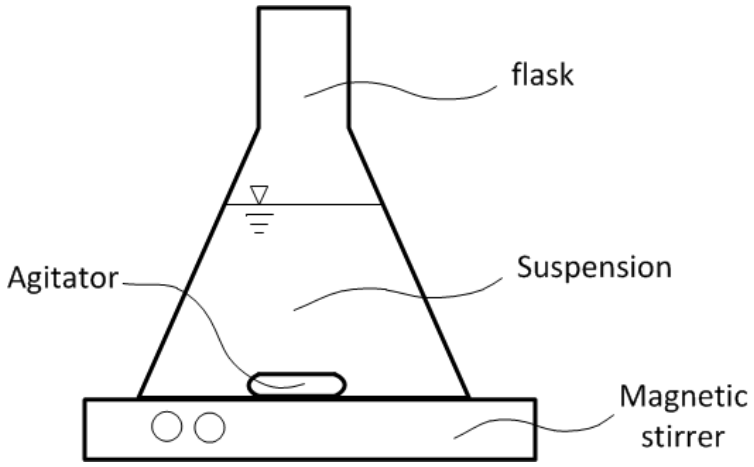

Figure 4.4: Setup for the adsorption kinetics experiments

To analyze the concentration change over time, samples of 5 mL were taken at different times. For the first two hours, samples were taken every 30 minutes, afterwards hourly or every two hours. After 8 hours the next sample was taken at 24, 48 and finally 72 hours. It was assumed that the container is ideally mixed so taking a sample of 5 mL would change the total mass but not the concentration of adsorbent or other compounds. Further the percentage of the total amount of sample taken was minimized by using 1L of suspension (in total 5.5% with a total amount of 11 samples). The samples were filtred with a Millipore filter with a diameter of 25 mm and a pore size of 0.22 μm. The supernatants were acidified with Nitric Acid (65%, Merck KgAa) to preserve the sample before analyzing them with atomic adsorption spectroscopy (see section 4.3.2).[60, 61]

4.2.3 Adsorption isotherms

After the experiments of the adsorption kinetics, the adsorption isotherms experiments were conducted. To get a better insight of the duration until state of equilibrium is reached, the results of the kinetics were evaluated. After 48 hours equilibrium was reached to a satisfactory point (see section 5.2) and so all isotherm experiments were carried out for 48 hours. Others authors report similar experiments times. [13, 62].
The setup for the batch experiments is shown in figure 4.5. Each flask contained 100 mL of solution and a certain amount of adsorbent which was varied to see the difference in adsorbed

metal. First the different amounts of adsorbent was measured weighted the balance and filled in the flasks using 0.01, 0.05, 0.075, 0.1, 0.15, 0.2, 0.25, 0.3 g and a blank which contained no hematite. The solution with a certain pH and ionic strength was added and the flasks were sealed with parafilm. Agitation was achieved by magnetic stirring. Each experiment was performed in duplicate at the same time (see figure 4.5) in order to have the same conditions on temperature and later be able to measure the concentration with the same calibration curve.

Figure 4.5: Setup of the adsorption isotherm experiments

The conducted experiments are shown in table 4.3, for example the experiments with Nickel included three batches with pH 7 (varying ionic strength by adding $NaNO_3$) and one with pH 5. The pH for nickel and lead was chosen by figure 4.6 as a maximum and minimum adsorption capacity. Further for chromium no such table was found and pH was chosen with the knowledge and insight of former works at the institute.

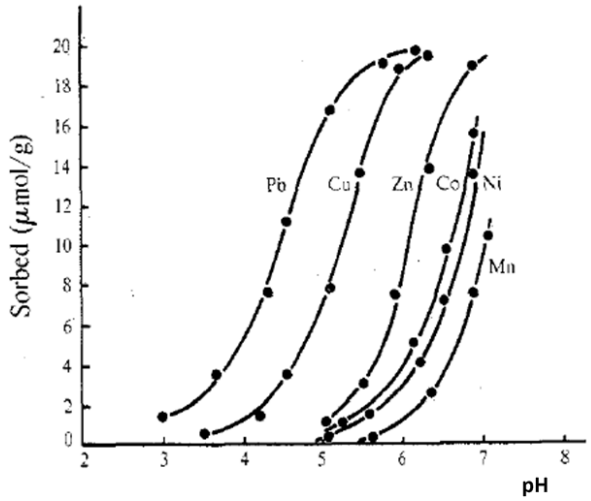

Figure 4.6: Adsorption capacities of different heavy metals (20 μmol/g) on hematite [63]

Table 4.3: Conditions of the adsorption isotherm experiments

Metal ion	pH	Ionic strength [mM]		
Cr(III)	5	1	10	100
Cr(VI)	5 8	1	10 10	100
Ni(II)	7 5	1	10 10	100
Pb(II)	6 5	1	10 10	100

After 48 hours samples were taken and filtred with a Millipore filter with a diameter of 25 mm and a pore size of 0.22 μm. The supernatants were acidified with Nitric Acid(65%, Merck KgAa) before analyzing them with atomic adsorption spectroscopy (see section 4.3.2).[60, 61] Further the pH of the final suspension was taken to see if the buffer worked and what influence the adsorption had.

4.3 Analytical methods

4.3.1 Surface area and pore measurement

To analyze the adsorbent in terms of surface area, Brunauer-Emmet-Teller (BET) N_2 method was used. Pore size distribution was calculated by the Barrett, Joyner and Halenda (BJH) N_2 adsorption/desorption method at 77K (see section 3.3.2) using the Coulter^{TM} SA 3100^{TM} analyzer.

Prior to the gas adsorption measurement an outgassing procedure has to be done in order to remove all gas molecules which are already attached to the surface and the actual dry sample mass has to be determined. This was done by using a clean and dry sample holder which was weighted as tare. The pre-dried sample was filled into the sample holder and attached to the analyzer.

Then the outgassing procedure began and the sample was evacuated for 180 min with a residual pressure p $<$ 0.133 Pa (1 mmHg) at 120°C. After cooling down the sample holder with sample to room temperature, it was weighted and the dry sample weight could be calculated.

The measurement itself was carried out with nitrogen as adsorptive gas and the adsorption temperature of 77K was achieved by plunging the sample into liquid nitrogen throughout the measurement. By measuring the pressure in the sample holder and knowing how much volume of nitrogen was introduced, the adsorbed volume can be calculated by using ideal gas law (see section 3.3.2).[64]

After collecting the data, the BET surface area and the Pore size were calculated by the Barrett, Joyner and Halenda (BJH) method (see section 3.3.2).

4.3.2 Atomic absorption spectroscopy

For the analysis of the taken samples from the adsorption experiments, atomic absorption spectroscopy was used as analyzing method. The samples were stored in glass ware and acidified.

To get the solutions for the calibration curves of each metal, standard solutions (Merck KgAa) were used. Those were for chromium $Cr(NO_3)_3$, for lead $Pb(NO_3)_3$ and for Nickel

$Ni(NO_3)_3$. All of them were in a solution of 0.5 mol/L of HNO_3. A 100 mg/L stock solution was prepared with whom the standard solutions of 2, 5, 7, 10 and 12 mg/L of each metal were prepared. RO-water was used as blank.
Before each measurement the lamp was warmed up and an optical configuration was carried out as well as an Autozero.
The wavelength, flow of the used gas composite and the background correction are shown in table 4.4.

Table 4.4: Configuration of the atomic absorption spectroscopy for the different metals

Metal	Wavelength [nm]	Gas mixture & flow [L/min]	Background corr.
Chromium	357.9	Nitrous oxide-acetylen; 4.2	D_2 quadline
Nickel	232	Air-acetylen; 0.9	D_2 quadline
Lead	217	Air-acetylen; 0.9	D_2 quadline

Each sample was measured three times and the average was taken automatically by the analyzer with giving the relative standard deviation (RSD).

4.3.3 Zeta potential and particle size

The device used was a Malvern Zetasizer ZS. With this analyzer the particle size of the hematite was investigated and the measurements of the zeta potential were obtained.
For the particle size, 100 mL of ultrapure water was mixed with 0.1 g of hematite to obtain a solution with a concentration of 1 g/L. This solution was mixed and put into the measure cell with a syringe of 10 mL. Then it was measured, cleaned and the same procedure was done again. Each sample was measured five times and three samples were tested.
For the eletrophoretic mobility measurements, the suspensions were prepared in a glassware container by mixing water and the tested salt and/or metal concentration according to the experimental conditions. The experiments were carried out like described in [65]. For each measurement 100 mL of solution was prepared and then mixed with 0.1 g of hematite to have a representative concentration of 1 g/L. After agitation for 30 minutes, the suspension was allowed to stand for 15 minutes to let the larger particles settle. Then the pH was fixed

depending on the suspension with 1M NaOH and 1M of HCl.
An aliquot from the suspension was slowly poured into the electrophoresis cell. The test cell was always conditioned with the test suspension before each measurement. Each sample was measured 10 times. The applied voltage was set automatically between 40-100 V and before each measurement the cell had an equilibrium time of 60 s. The temperature in the cell was adjusted to 20°C. The Smoluchowski model was used where $f(Ka)$ is 1.5.
The pH range tested for each metal and without metal was set from $4-10$ which covers the appearance of natural waters.

4.3.4 Miscellaneous equipment

The balance used in this work was a Denver Instruments APX-200 with a total range of 200 g and steps of 0.1 mg ±0.2 mg.
Further the pH meter used was a Denver Instruments UB-10 Ultra-Basic with a pH range from 0-14 and a resolution of 0.01 pH ± 0.1.
The samples were taken and stored in glassware of 10 mL, all solutions and suspensions were prepared in glassware, as well as the experiments were performed in Erlenmeyer flasks.

5 Results and discussion

In this part results are presented following the project structure. Pursuing the goal of obtaining the adsorption kinetics and isotherms of Cr(III), Cr(VI), Ni(II) and Pb(II) followed by identifying them with suitable models.
The project steps were carried out as follows:

1. Hematite was synthesized in the laboratory and characterized.

2. Adsorption kinetic experiments were carried out to obtain the kinetics and the time of equilibrium.

3. Adsorption isotherm experiments were determined and compared to mathematical models.

4. Zeta potential measurements were performed to get a better insight of adsorption phenomena, e.g. surface charge.

5.1 Characterization of the adsorbent

5.1.1 Specific surface and pore analysis

In figure 5.1 the adsorption/desorption isotherm of N_2 for hematite is shown. The isotherm exhibit a sharp but very short increase in nitrogen adsorbate at low relative pressure between about 0 and 0.01 p/p_0. The inflection point, the knee of the isotherm, occurs around 0.01 - 0.02 p/p_0 and indicates the stage at which monolayer coverage is complete.
For $0.05 < p/p_0 < 0.8$ only a very low uptake of adsorbate can be observed which results in an almost plateau of the isotherm. That indicates micropore filling is completed and just a low multilayer adsorption occurs in this range. In the last range between $0.8 < p/p_0 < 0.95$ the adsorption is increasing but still far lower than in the initial part of the isotherm. Also a hysteresis loop can be observed at the isotherm in this pressure range which is associated with the occurrence of pore condensation and indicates mesoporous materials.
The type of isotherm obtained can be seen as one of type IV described in section 3.2.5. Looking more detailed at the hysteresis loop, it can be identified most likely as a H1 type of loop (see section 3.2.5) where the horizontal distance stays more or less the same over the relative pressure. This indicates well defined cylindrical pore channels.

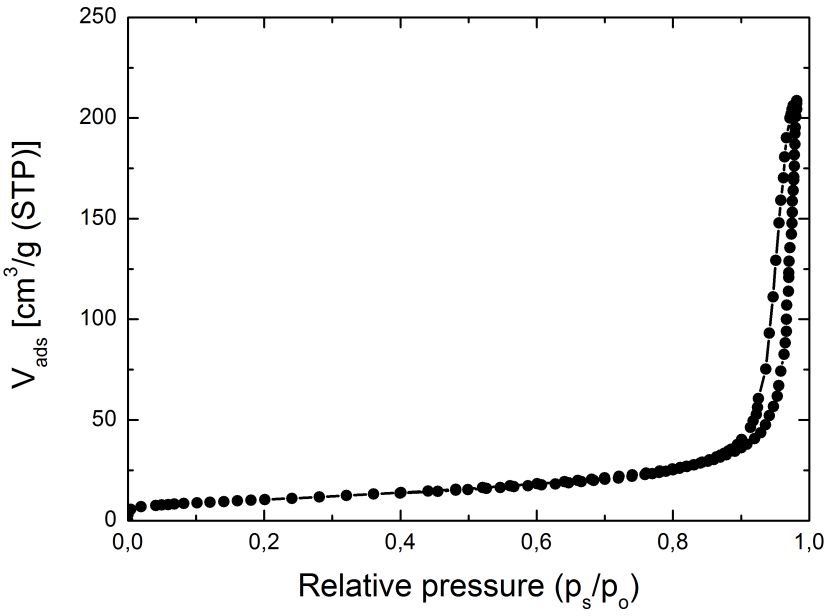

Figure 5.1: BET isotherm of hematite (N_2 method)

The pore size distribution was calculated by the BJH method (see section 3.3.2) and in table 5.1 the two results for adsorption and desorption are shown. Differences between adsorption and desorption result from discrepancies between adsorbate structure and the model of open-ended cylindrical capillaries. Less than 10% of the pores are smaller than 20 nm. The main part of the particles are in a size range between $20 - 80$ nm or bigger.

Table 5.1: BJH pore size distribution (adsorption and desorption)

Pore diameter range [nm]	**Pore volume [mL/g]**	**%**
Adsorption		
Under 6	0.00573	1.82
6 - 20	0.01933	6.31
20 - 80	0.19704	62.44
Over 80	0.09289	29.43
Desorption		
Under 6	0.00136	0.41
6 - 20	0.02019	6.12
20 - 80	0.29619	89.55
Over 80	0.01300	3.93

The specific surface area was calculated by the BET method and resulted in a value of $37.54 m^2$/g. Further the pore volume was calculated to be 0.3160 mL/g.
The obtained C value in this measurement was 105.942 which is > 100 and therefore a sign of a well-defined localized monolayer for low-temperature adsorption (e.g. at 77 K).[30]
Compared to values in the literature the BET value of the specific surface is rather above average. There are specific surfaces reported for hematite rich soils between 10-36 m^2/g [66], hematites produced from a solution at temperatures at or around 100°C ranging from $10-90$ m^2/g [67] and hematite prepared by the sol-gel method with a specific surface of 12.4 m^2/g [68].

5.1.2 Particle size

The particle size measurement was done with dynamic light scattering. Three different suspensions of 1 g/L hematite and water were measured five times each. The measurements turned out to be quite unstable and it seemed that the samples were sedimenting rapidly. Due to that fact, the analyzer identified only two measurements of the same sample as qualitatively acceptable which are shown in figure 5.2.
Three peaks are recognized: the first at 185.2 nm with a volume percentage of 6.9%, the second at 960.2 nm with 27% and the biggest at 4855 nm with 66.1%. The average particle size diameter calculated is 337 nm with a count rate of 358 kcps.

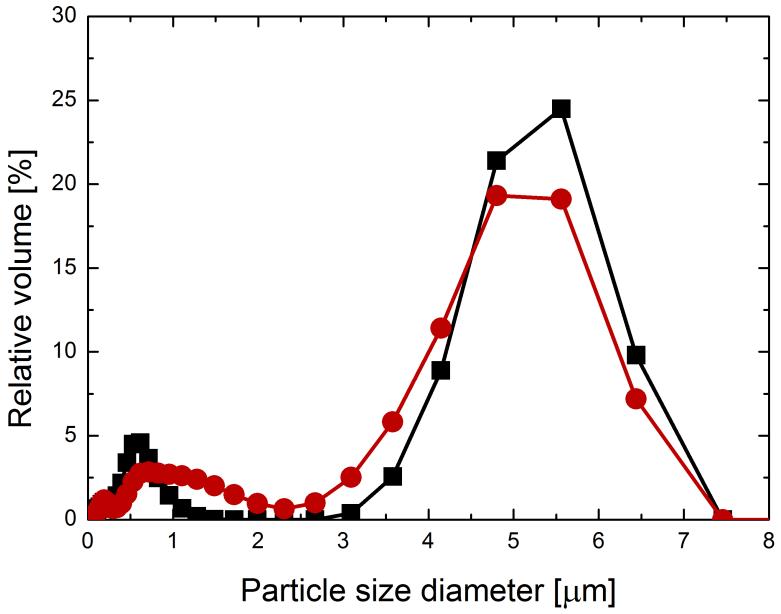

Figure 5.2: Particle size diameter distribution for hematite by dynamic light scattering(two measurements of the same sample); experimental conditions: hematite concentration, 1 g/L; temperature, 20°C

5.1.3 X-ray diffraction

The X-ray diffraction was done in the Civil and Environmental Engineering Department, University of Missouri, USA. The sample was sent and analyzed. The results were compared to a standard hematite X-ray diffraction pattern [69] and are shown in figure 5.3. The

pattern and the sample show the same characteristic peaks except the one at around 24°.

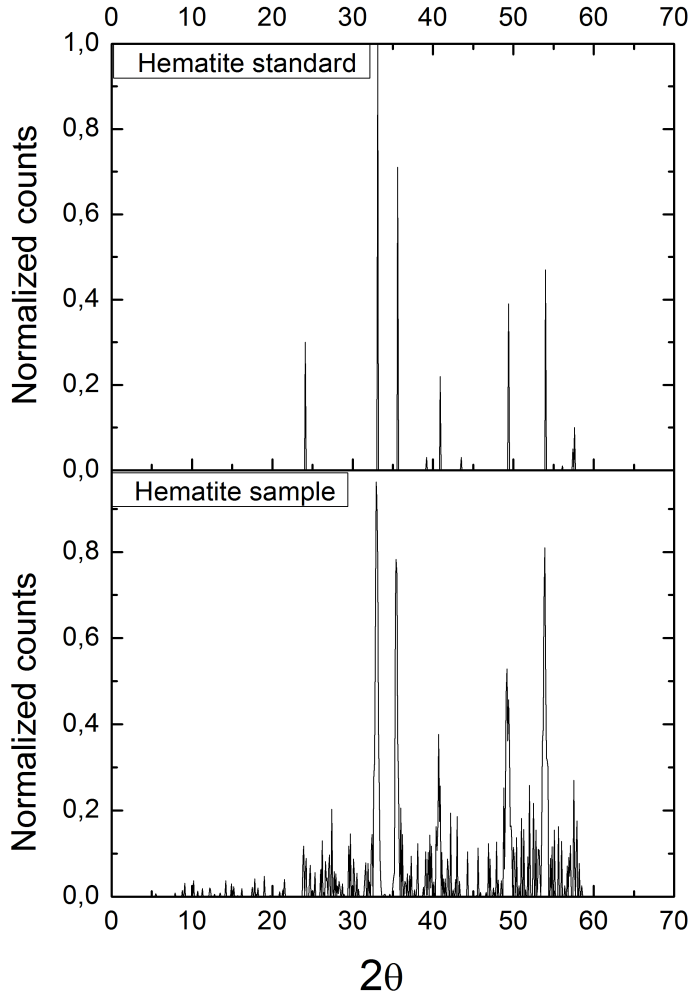

Figure 5.3: X-ray diffraction of hematite sample and a standard pattern

5.2 Adsorption kinetics

The adsorption kinetics experiment were conducted one time and then evaluated for each metal.

Three models (pseudo-first, pseudo-second order and Elovich models) are fitted to the values. Each model was linearized like described in section 3.2.4 so the parameters could obtained and are shown in the tables for each metal including the R^2 value for each model. For the pseudo-first order model, an iteration was used to maximize R^2 by changing Q_e. No partial fitting was tried since the pseudo-second order model shows a good compliance over the observed range regarding the R^2 value. However, it seems like the Elovich model fits better when plotted in all of the investigated metals. That might be because the transformation to a linearized model can result in a structural error, respectively the R^2 value is not the best function to represent the error (also see section 5.3). All of the kinetics show a fast adsorption in the beginning followed by a slow phase until reaching equilibrium. This kind of rapid adsorption and reaching high percentages of the final adsorption value of different metals after a few days adsorbed by hematite is also reported by [70].

Further in [71], the adsorption kinetics for metals onto hematite are modeled and it is assumed that the reason for the fast adsorption in the beginning is a fast outer-sphere complexation followed by a slow inner-sphere complexation.

5.2.1 Chromium(III)

The Cr(III) kinetic results are shown in figure 5.4.

In the beginning of the adsorption the kinetics are very fast and after only 2 hours, more than 65% of the final value (modeled Q_e) are already adsorbed. The maximum loading of adsorbate was measured after 56 hours with a value of 7.59 mg Cr(III)/g hematite. The highest R^2 was achieved by the pseudo second-order model with a value of 0.998.

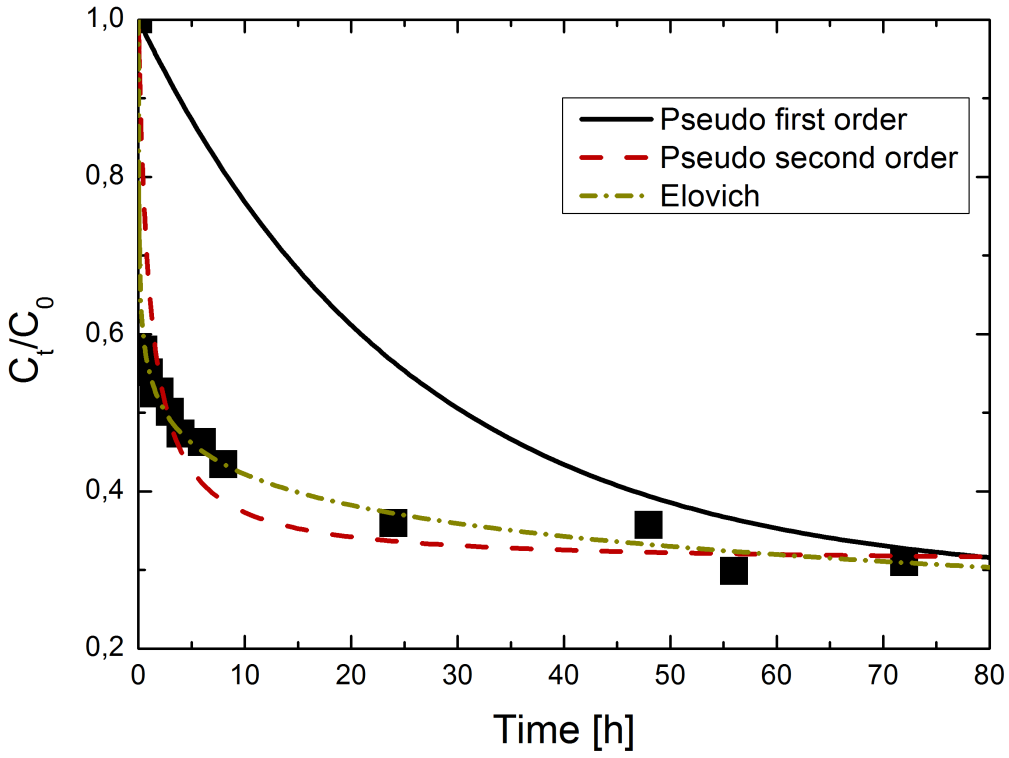

Figure 5.4: Comparison of pseudo-first-, pseudo-second-order and Elovich kinetic models of Cr(III) adsorption onto hematite. Experimental conditions: initial Cr(III) concentration, 10.83 mg/L; concentration of adsorbent, 1 g/L; pH 5.25 - 0.7; 10 mM $NaNO_3$; temperature, $25 \pm 3°C$

After 48 hours more than 97% of the final value Q_e are reached regarding the pseudo-second order model. So this time was taken as a reference for a reached state of equilibrium to conduct the isotherm results.

Table 5.2: Parameters for the different fitted models of Cr(III) kinetics

Model	Parameter 1	Parameter 2	R^2
Pseudo-first order	$k_1 = 0.039$	$Q_e = 7.748$	0.827
Pseudo-second order	$k_2 = 0.128$	$Q_e = 7.496$	0.998
Elovich	$\alpha = 1559.8$	$\beta = 1.619$	0.980

5.2.2 Chromium(VI)

Cr(VI) adsorbs fast on hematite. As seen in figure 5.5, there is a drop at the beginning and then the concentration in the solution slowly decreases. After half an hour already more than 80% of the final adsorption value are reached.

The maximum loading of adsorbate was measured after 56 hours with a value of 3.38 mg Cr(VI)/g hematite. This is significantly lower than the value for Cr(III).

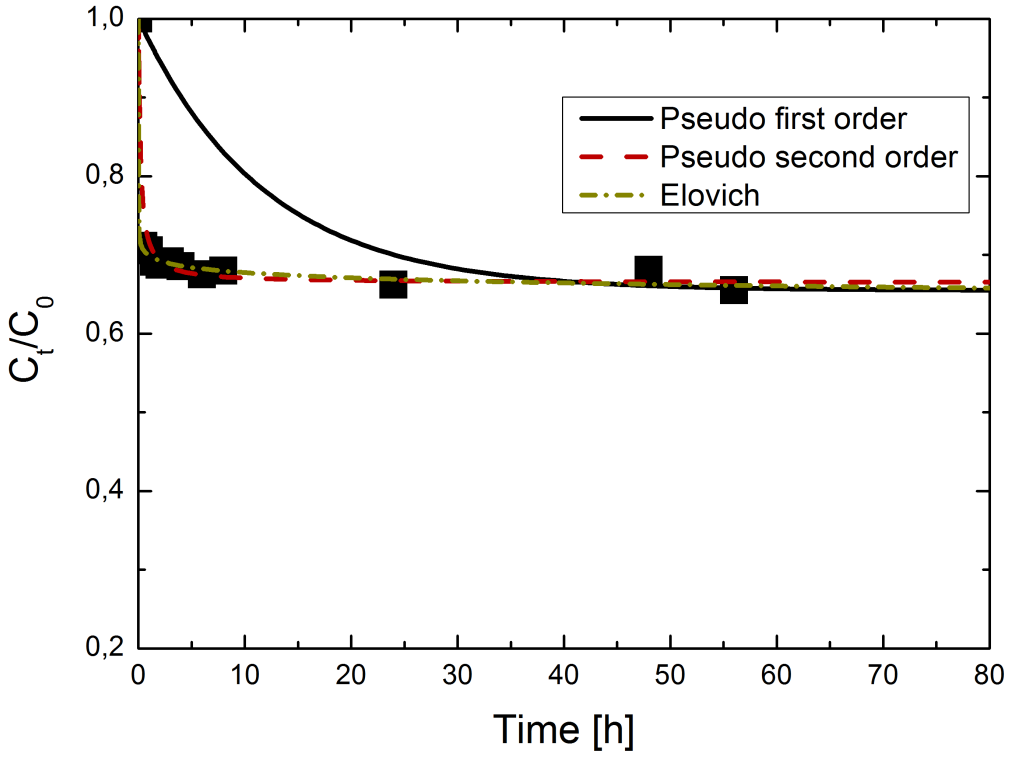

Figure 5.5: Comparison of pseudo-first-, pseudo-second-order and Elovich kinetic models of Cr(VI) adsorption onto hematite. Experimental conditions: initial Cr(VI) concentration, 9.979 mg/L; concentration of adsorbent, 1 g/L; pH 4.93 ± 0.1; 10 mM $NaNO_3$; temperature, $25 \pm 3°C$

Table 5.3: Parameters for the different fitted models of Cr(VI) kinetics

Model	Parameter 1	Parameter 2	$\mathbf{R^2}$
Pseudo-first order	$k_1 = 0.0845$	$Q_e = 3.380$	0.588
Pseudo-second order	$k_2 = 1,662$	$Q_e = 3.284$	0.998
Elovich	$\alpha = 5.77 \cdot 10^{12}$	$\beta = 10.787$	0.784

The best compliance with a model by numbers has the Pseudo-second order model which achieves a value of R^2 of 0.998 and a calculated Q_e of 3.284. The state of equilibrium seems to be reached after about 10 hours when the concentration stabilize and the difference are in the range of measure accuracy.

5.2.3 Lead

The adsorption of Pb follows the same scheme as the metals before (especially Cr(VI)) with a huge drop in the first half hour and then a continuous slow decrease till reaching state of equilibrium. That said, the maximum amount adsorbed was measured after 50 hours with a value of 4,61 mg Pb/g hematite. After half an hour over 80% of the final amount are already adsorbed and an acceptable state of equilibrium is reached after about 10 hours when the concentration in the solution continues only to decreases very slowly.

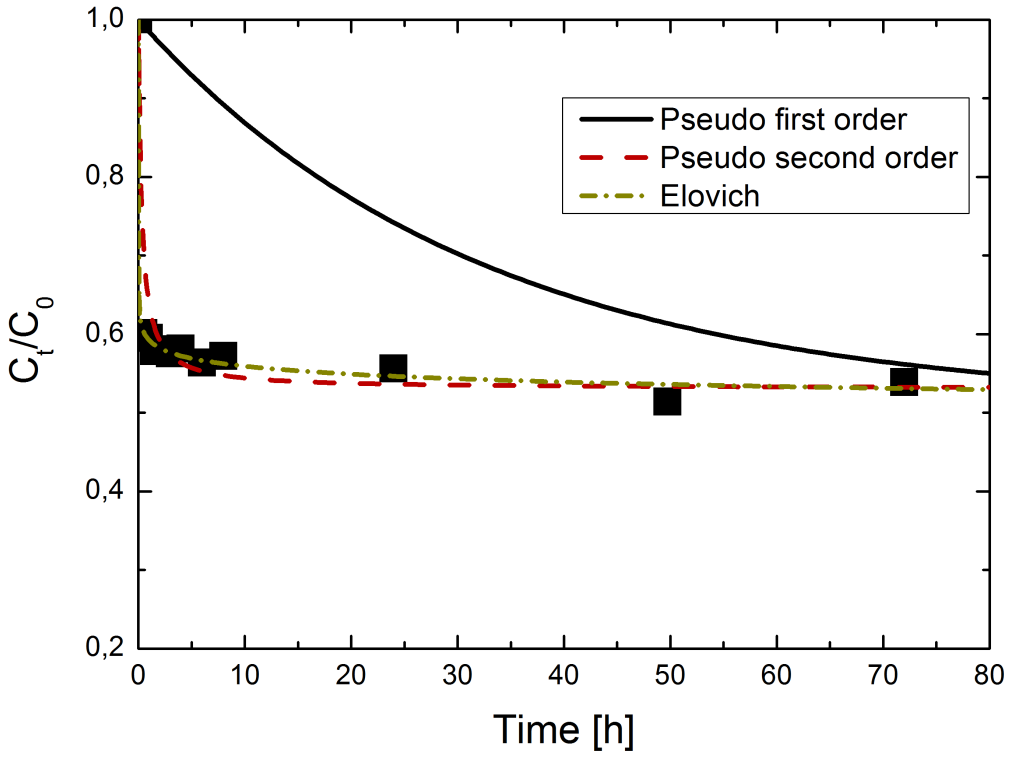

Figure 5.6: Comparison of pseudo-first-, pseudo-second-order and Elovich kinetic models of Pb adsorption onto hematite. Experimental conditions: initial Pb concentration, 9.476 mg/L; concentration of adsorbent, 1 g/L; pH 4.97 ± 0.1; 10 mM $NaNO_3$; temperature, $22 \pm 2°C$

The best fitting model for the adsorption kinetics of Pb is found to be the pseudo-second order model which has a R^2 of 0.999 and a calculated Q_e of 4.45. However, the Elovich model seems to be adequate too regarding the plot in figure 5.6 although the R^2 value only achieves 0.853.

Table 5.4: Parameters for the different fitted models of Pb kinetics

Model	Parameter 1	Parameter 2	R^2
Pseudo-first order	$k_1 = 0,0311$	$Q_e = 4,649$	0.465
Pseudo-second order	$k_2 = 0,744$	$Q_e = 4,448$	0.999
Elovich	$\alpha = 2,37 \cdot 10^{11}$	$\beta = 7,299$	0.853

5.2.4 Nickel

The Ni kinetic results are shown in figure 5.7.

In the beginning of the adsorption the kinetics are very fast and after only 2 hours, more than 50% of the final value (modeled Q_e) are already adsorbed. The maximum loading of the adsorbate was measured after 72 hours with a value of 4.49 mg Ni/g hematite. The last value measured after 72 hours shows a slight drop compared to the value after 48 hours. This could indicate that the adsorption continues to decrease although the 24 hours before no difference in the concentration could be observed or there was a slight deviation due to the measuring.

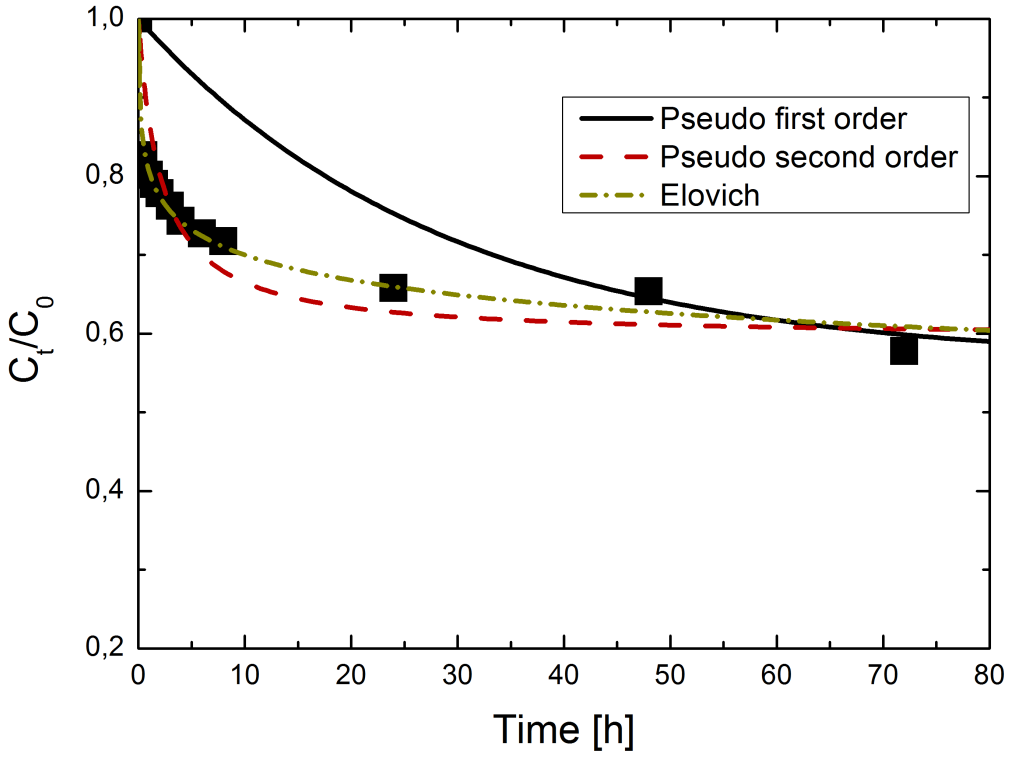

Figure 5.7: Comparison of pseudo-first-, pseudo-second-order and Elovich kinetic models of Ni adsorption onto hematite. Experimental conditions: initial Ni concentration, 10.622 mg/L; concentration of adsorbent, 1 g/L; pH 6.96 ± 0.2; 10 mM $NaNO_3$; temperature, $22 \pm 2°C$

Table 5.5: Parameters for the different fitted models of Ni kinetics

Model	Parameter 1	Parameter 2	R^2
Pseudo-first order	$k_1 = 0,0348$	$Q_e = 4,642$	0.8721
Pseudo-second order	$k_2 = 0,111$	$Q_e = 4,307$	0.987
Elovich	$\alpha = 32,690$	$\beta = 2,0412$	0.965

The best compliance with a model by numbers has the Pseudo-second order model which achieves a value of R^2 of 0.987 and a calculated Q_e of 4.307. Also the Elovich has a high R^2 value of 0.965 and seems to fit better than the pseudo-second order plot (see figure 5.7). The state of equilibrium seems to be reached after about 48 hours although the last measured value is almost 20% lower. However this could be due to a measuring deviation which is supported by the fact that the decrease between 24 and 48 hours is almost zero, respectively positive. Other studies also show an increase in adsorption of Ni on goethite after extending the observed time from 2 h to 42 days.[72] The cation adsorption starts rapidly and is followed by a slow adsorption. This phenomena was explained by a rapid adsorption on the external surfaces and the a slow diffusion process into the particles.

Summary and Conclusion

- In all four different investigated models the pseudo-second order model achieves the highest R^2 values regarding the adsorption kinetics. However, the Elovich plot seems to fit at least equal or even better regarding the figures shown.
- After 48 hours, it seems that an acceptable state of equilibrium is reached for all metals. Therefore 48 hours is set to be the investigated time for all following adsorption isotherm experiments in which it is assumed that state of equilibrium is reached.
- Eventually further investigation should be done with the adsorption kinetics of Nickel since the last value dropped by almost 20% compared to the value 24 hours before.

5.3 Adsorption isotherms

The experiments of the adsorption isotherms were carried out for 48 hours and conducted twice for each setup (see section 4.2.3). For each metal there is a figure that compares the two base case experiments (10 mM $NaNO_3$ as ionic strength) in terms of pH variation and differences in adsorbed metal per mass of hematite over the concentration in the solution. Further one figure shows the best model for the adsorption isotherms and the influence of the ionic strength. Although in [10], no influence on the adsorption of heavy metal cations is reported by $NaNO_3$, chromium(III) and lead show a significant decrease with higher concentration of $NaNO_3$.
Finally for chromium(VI), nickel and lead another pH was tested and compared with the base case.
The amount of metal adsorbed to the hematite Q_e was calculated with equation 5.1 where C_0 is the measured concentration of the metal in the blank [mg/L], C_e the measured concentration of the metal in one of the adsorption experiments [mg/L], V the volume of solution used [L] and m_H the mass of the hematite [g].

$$Q_e = \frac{(C_0 - C_e)V}{m_H} \tag{5.1}$$

The plots of chromium(III) (see figure 5.8), Nickel (see figure 5.19) and parts of Lead (see figure 5.15) show a big increase of metal adsorbed in the experiment with the lowest concentration of hematite (0.1 g/L). These big leaps do not seem to be the result of bigger adsorption properties because there is no satisfying explanation by adsorption phenomena. Further the percental error rises with smaller differences between the measured concentrations and with lower masses of adsorbent. However the calculated Q_e of a hematite concentration of 0.1 g/L almost always exceeded the expected values which can not be explained only by an error of measurement. This lead to an exclusion of the last point for the modeling of the isotherms although they are shown in the comparison of the two conducted batches.

For the modeling the presented linearizations from section 3.2.5 were used and the R^2 values were compared. It seemed that the Temkin model always showed slightly lower compliance

than the other two models and so only plots of Freundlich or Langmuir are shown although all parameters were calculated and also shown in the tables in each section. Further the Temkin model is often negative in the beginning until the factor $A_T \cdot C_e$ reaches 1 so the logarithm of this factor reaches 0.

In addition a simple linear model was tried to fit the experimental data and also showed very good compliance in the range of the data. The models did not go through the origin so physically it makes no sense but could be used in a certain range as a first and simple approximation.

During the calculations the linearization of the Langmuir isotherm was changed to equation 5.2 in order to obtain better constants. This was done because in some experiments the C_e reached 0 and dividing by 0 lead to problems. It is notable that between the linearizations can be significant differences regarding the constants and the R^2 values.[73]

This is because each of these transformations changes the original error distribution (for better or worse). The best transformation is not necessarily that which gives the highest correlation coefficient but rather that in which the resulting error distribution most closely matches the "true" error distribution. [74]

Another possibility to determine the parameter is to use non-linear regression and choose an error function in order to maximize the match of results and model.[46] However in this work only linear regression was used.

$$\frac{C_e}{Q_e} = \frac{C_e}{Q_{max}} + \frac{1}{Q_{max} b} \tag{5.2}$$

5.3.1 Chromium(III)

Figure 5.8 compares the two same base case experiments with each other. The buffer could not maintain the pH and so it dropped down to up to 4.2 in the flask with the highest concentration of hematite. Even in the blank which contained no hematite, the pH dropped as it was set to 5.0 before the experiment and 48 hours later it went down to 4.85, e.g 4.6.

The isotherms seem to be almost linear except the last point which jumps to a very high level and was discussed earlier. The maximum Q_e measured is 10.36 mg/g at a C_e of 6.36 mg/L (the point of 0.1 g/L hematite is excluded).

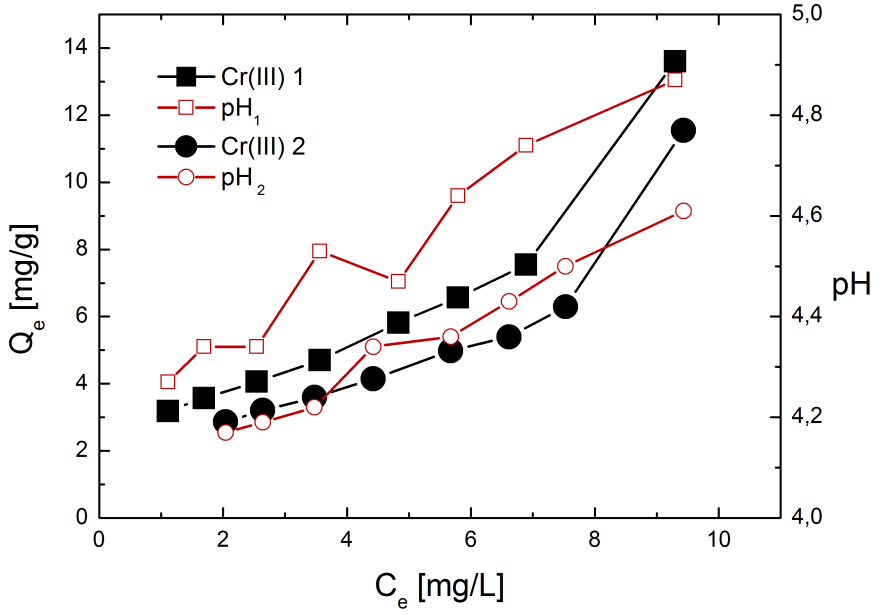

Figure 5.8: Isotherms Cr(III) and pH measured after experiments; experimental conditions: initial Cr(III) concentration, Batch 1: 10.66 mg/L, Batch 2: 10.89 mg/L; pH blank 1: 4.92, pH blank 2: 4.68; 10 mM $NaNO_3$; temperature, $21 \pm 3°C$

The best fit for the experimental data of Cr(III) was the Freundlich model as you can see in table 5.6 regarding R^2 values with values between 0.939 and 0.960. Also the other models show values around 0.9 which indicates that there should be more experiments with a wider range of points tested. The Freundlich model was used to fit the experimental data of Cr(III) at different ionic strength and pH 5 (shown in figure 5.9). It seems to fit well for all three tested conditions. However there is a tendency that the point with the highest concentrations tends to be higher than the others. The lower the ionic strength, the higher the maximum Q_e calculated from the Langmuir model shown in table 5.7. However the plot of the model for the 10 mM and the 100 mM cross each other at a fluid concentration of chromium at around 3 mg/L. So below that point 100 mM model has higher Q_e values than the 10mM model. The salt concentration has an important influence on the adsorption of Cr(III), especially at high metal concentrations in the solution.

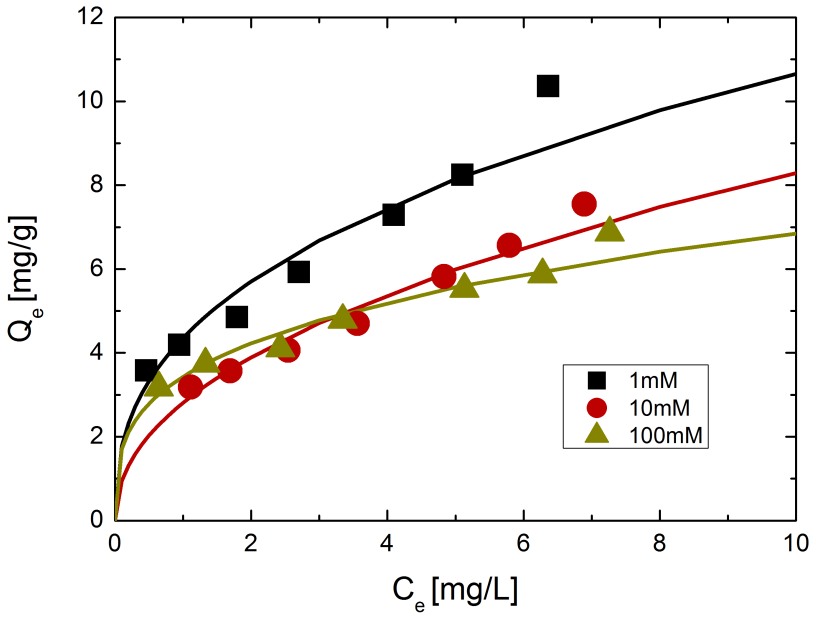

Figure 5.9: Freundlich model fitted to isotherm experiments (Batch 1) of Cr(III) with different ionic strengths (1, 10, 100 mM $NaNO_3$) and pH 5; Experimental conditions: initial Cr(III) concentration, 1 mM: 11.53 mg/L; 10 mM: 10.66 mg/L; 100 mM: 10.67 mg/L

Table 5.6: R^2 values for the different fitted isotherm models of Cr(III) with different ionic strengths ($NaNO_3$)

Cr(III) Case	Freundlich	Langmuir	Temkin
pH 5, 1 mM	**0.939**	0.895	0.852
pH 5, 10 mM	**0.960**	0.908	0.907
pH 5, 100mM	**0.952**	0.957	0.898

Table 5.7: Parameters for the different fitted isotherm models of Cr(III) with different ionic strengths ($NaNO_3$)

Cr(III) Case	Freundlich		Langmuir		Temkin	
	K_f	n	Q_{max} [mg/g]	b	A_T	b_T [kJ/mol]
pH 5, 1 mM	4.35	2.57	**12.08**	0.48	6.63	1.04
pH 5, 10 mM	2.81	2.12	**10.52**	0.29	2.81	1.06
pH 5, 100mM	3.43	3.32	**7.58**	0.65	11.29	1.62

5.3.2 Chromium(VI)

The comparison of the base cases of Cr(VI) in figure 5.10 shows two very similar plots for Q_e and only small differences for the pH. The last point jumps slightly for the first batch but not as extreme as with Cr(III). However, the maximum adsorption is lower for Cr(VI) than Cr(III) and seems to have reached the maximum adsorption Q_e because the plots are almost constant. The maximum Q_e measured is 2.88 mg/g at a C_e of 9.26 mg/L (the point of 0.1 g/L hematite is excluded).

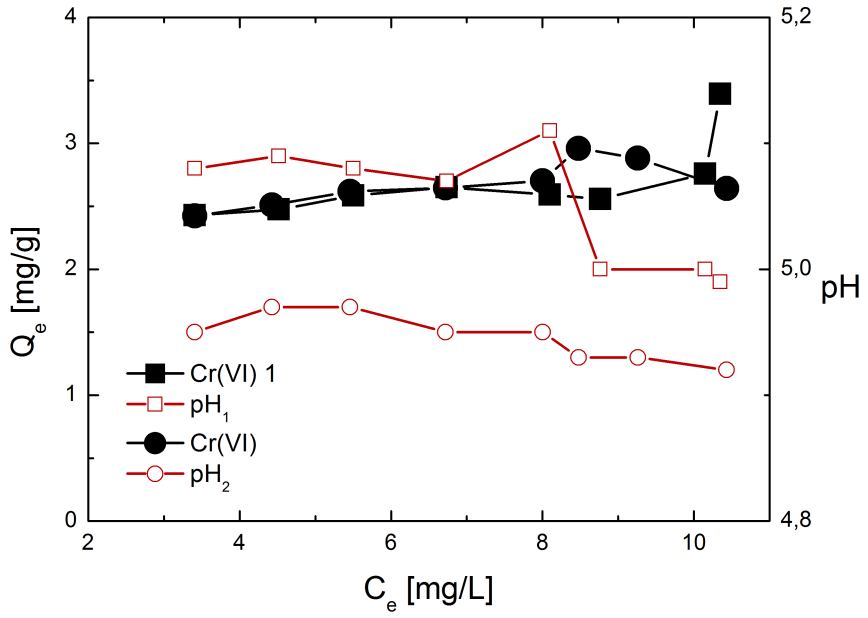

Figure 5.10: Isotherms Cr(VI) and pH measured after experiments; experimental conditions: initial Cr(VI) concentration, Batch 1: 10.69 mg/L, Batch 2: 10.89 mg/L; pH blank 1: 5.03, pH blank 2: 4.91; 10 mM $NaNO_3$; temperature, $21 \pm 3°C$

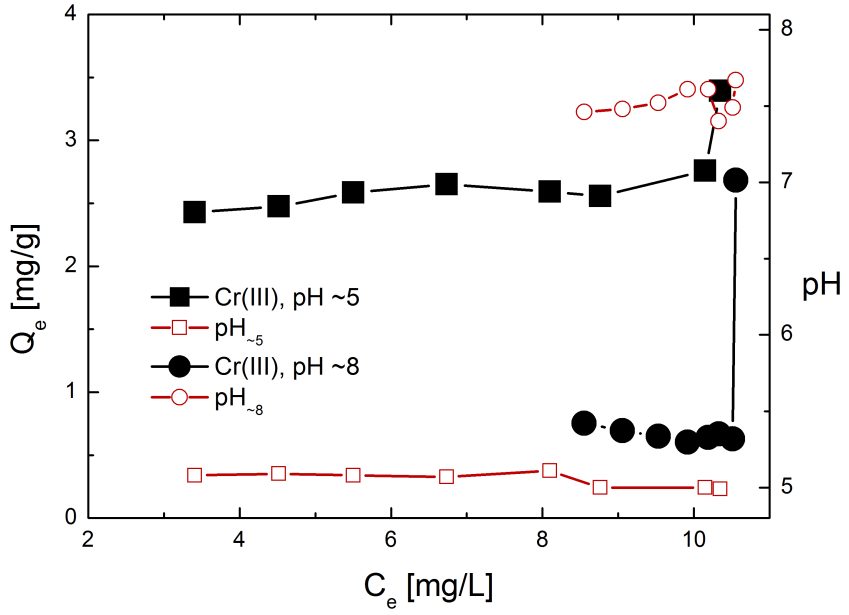

Figure 5.11: Comparison of Isotherms of Cr(VI) at pH 5 and 8; experimental conditions: initial Cr(VI) concentration, pH 5: 10.69 mg/L, pH 8: 10.89 mg/L; pH of blank, pH 5: 4.94, pH 8: 7.75; 10 mM $NaNO_3$; temperature, $21 \pm 3°C$

The best model fit to the results is the Langmuir model with the highest R^2 values shown in table 5.8. Two models were fitted to the experimental results of the Cr(VI) experiments with different ionic strength at pH 5: the Freundlich (shown in figure 5.13) and the Langmuir (shown in figure 5.14). The Freundlich model shows a very steep, almost vertical slope at the beginning and then turns more horizontal. The Langmuir model has a slightly smaller gradient in the beginning. Both fit the data well but more points in a lower C_e region would help to determine the exact behavior there.

The ionic strength has only a small influence on the adsorption and the differences in the maximum adsorption concentration are low (see table 5.9).

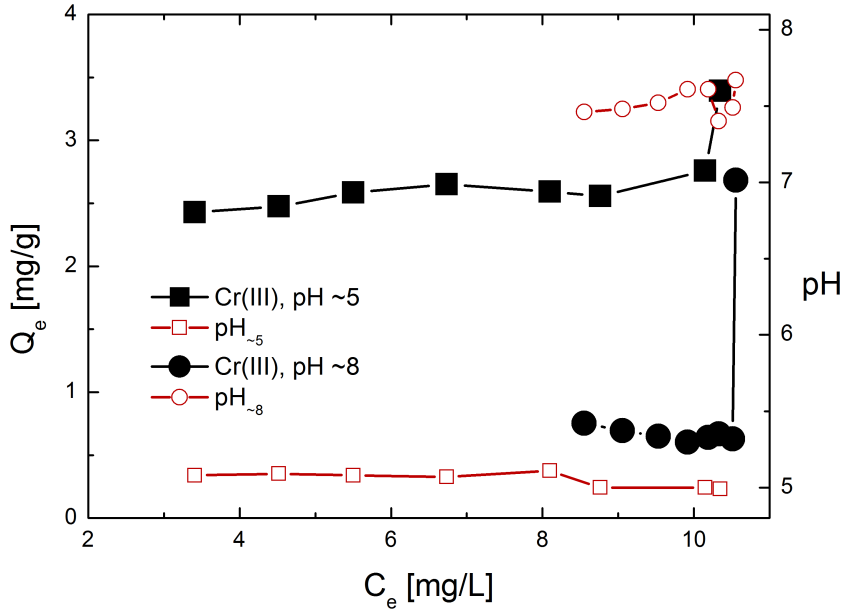

Figure 5.12: Comparison of Isotherms of Cr(VI) at pH 5 and 8; experimental conditions: initial Cr(VI) concentration, pH 5: 10.69 mg/L, pH 8: 10.89 mg/L; pH of blank, pH 5: 4.94, pH 8: 7.75; 10 mM $NaNO_3$; temperature, $21 \pm 3°C$

In figure 5.12 the adsorption capacity is compared at pH 5 and pH 8 with an ionic strength of 10 mM $NaNO_3$ each. The lower pH is pretty constant and the pH at 8 dropped down to around 7.5. This is due to the buffer range which is not ideal at pH 8. At pH 8 the adsorption capacity is very low compared to pH 5. This is in compliance with other works like [75] which investigated hydrous iron oxides and found to be the best range of the pH for the adsorption of hexavalent chromium the range between 3-6. Higher than that if falls off rapidly. Both fits seem to have reached a maximum load of adsorbate and thus the plots are almost constant. So for more detailed isotherms, a higher concentration range should be measured.

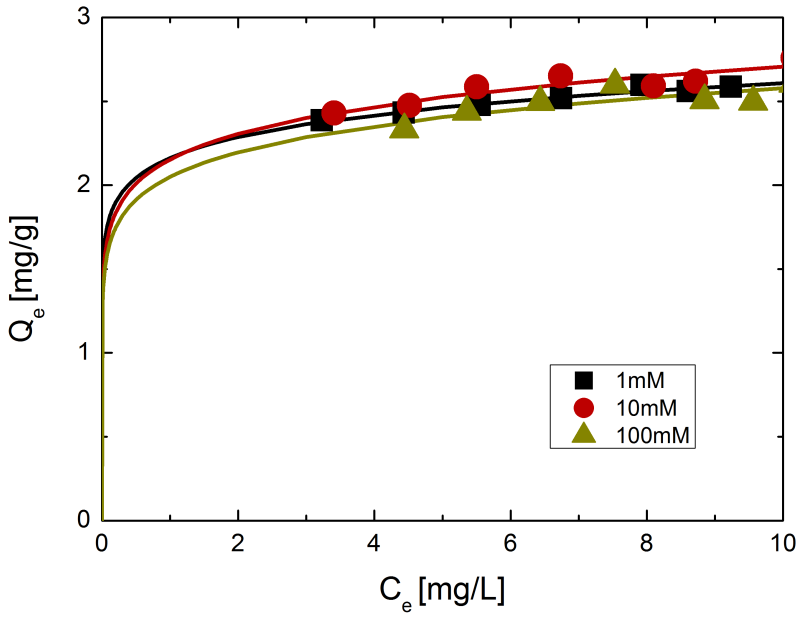

Figure 5.13: Freundlich model fitted to isotherm experiments (Batch 1) of Cr(VI) with different ionic strengths (1, 10, 100 mM $NaNO_3$); Experimental conditions: initial Cr(VI) concentration, 1 mM: 10.52 mg/L; 10 mM: 10.69 mg/L; 100 mM: 11.45 mg/L

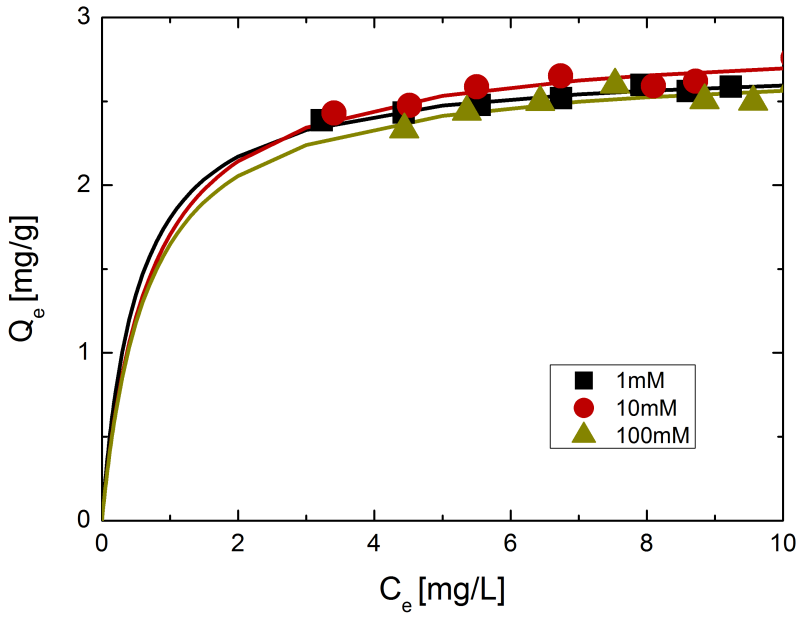

Figure 5.14: Langmuir model fitted to isotherm experiments (Batch 1) of Cr(VI) with different ionic strengths (1, 10, 100 mM $NaNO_3$); Experimental conditions: initial Cr(VI) concentration, 1 mM: 10.52 mg/L; 10 mM: 10.69 mg/L; 100 mM: 11.45 mg/L

Table 5.8: R^2 values for the different fitted isotherm models of Cr(VI) with different ionic strengths ($NaNO_3$)

Cr(VI) Case	Freundlich	Langmuir	Temkin
pH 5, 1 mM	0.949	**0.999**	0.946
pH 5, 10 mM	0.832	**0.996**	0.825
pH 5, 100mM	0.862	**0.913**	0.841

Table 5.9: Parameters for the different fitted isotherm models of Cr(VI) with different ionic strengths ($NaNO_3$)

Cr(VI) Case	Freundlich		Langmuir		Temkin	
	K_f	n	Q_{max} [mg/g]	b	A_T	b_T [kJ/mol]
pH 5, 1 mM	2.16	12.29	**2.73**	1.95	38331	12.11
pH 5, 10 mM	2.15	10.06	**2.88**	1.45	3918	9.56
pH 5, 100mM	2.05	10.03	**2.73**	1.52	2.02	2.29

5.3.3 Lead

Comparing the two base cases of lead with pH 6 in figure 5.15 shows a very good adsorption and a similar plot for both experiments. The in the calculation excluded points (highest C_e concentration) differ and it seems that the point of batch 2 with the higher Q_e is more realistic than the point of batch 1.

The pH of both experiments are pretty constant, only batch 1 drops slightly at high hematite concentrations. The maximum Q_e measured is 12.59 mg/g at a C_e of 3.01 mg/L (the point of 0.1 g/L hematite is excluded). Lead seems to be adsorbed really well and so the three points with the highest hematite concentrations (0.2 g, 0.25 g, 0.3 g) contain no more lead in the solution.

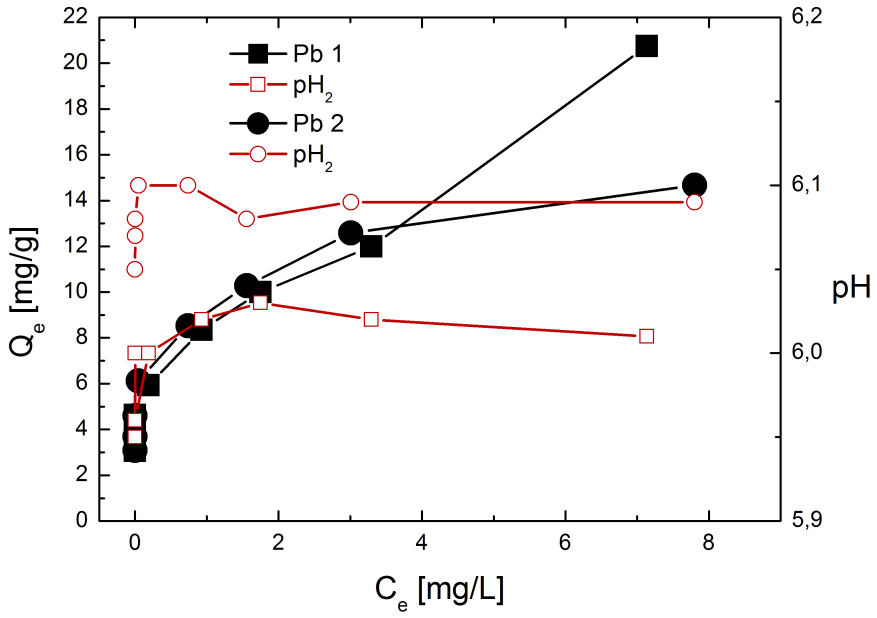

Figure 5.15: Isotherms Pb and pH measured after experiments; experimental conditions: initial Ni concentration, Batch 1: 9.25 mg/L, Batch 2: 10.25 mg/L; pH blank 1: 6.02, pH blank 2: 6.10; 10 mM $NaNO_3$; temperature, $19 \pm 2°C$

Further the adsorption of lead at pH 5 and pH 6 was compared. For both the pH was constant over the whole range of hematite concentrations. However the adsorption at pH 6 is much higher than at pH 5. At pH 6 three samples contained no more lead and the maximum adsorption was more than 12 mg/g at a C_e of 3.01 mg/L compared to a maximum adsorption at pH 5 of 4.54 mg/g at a C_e of 7.54 mg/L. This is in compliance with [63] which reports a strong adsorption edge meaning that in a small range of pH the adsorption changes significantly. Figure 4.6 shows this edge for lead amongst other metals.

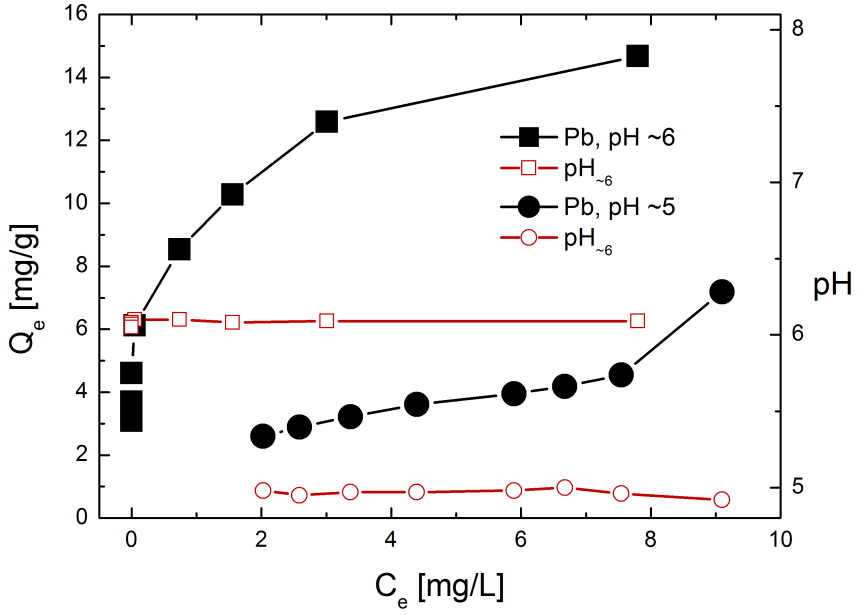

Figure 5.16: Comparison of Isotherms of Pb at pH 5 and 6; experimental conditions: initial Pb concentration, pH 5: 9.82 mg/L, pH 6: 10.25 mg/L; pH of blank, pH 5: 5.01, pH 6: 6.10; 10 mM $NaNO_3$; temperature, $19 \pm 3°C$

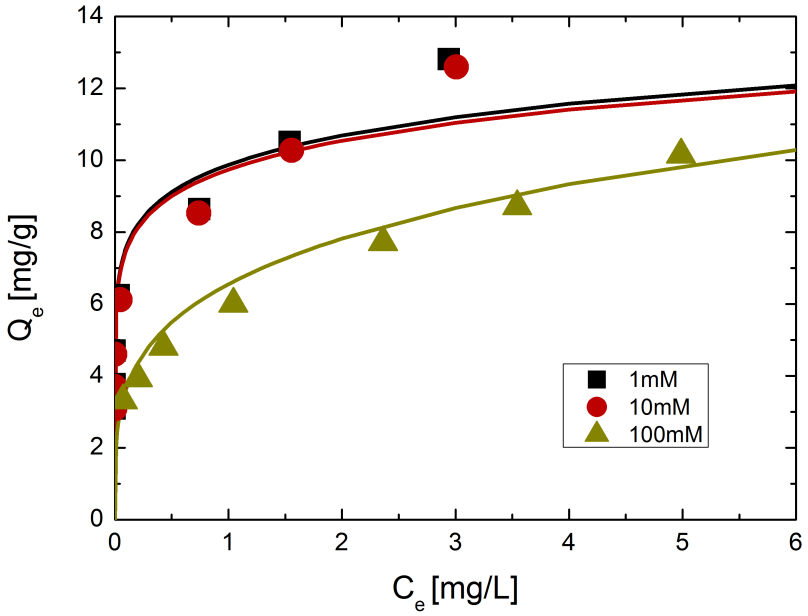

Figure 5.17: Freundlich model fitted to isotherm experiments (Batch 1) of Pb with different ionic strengths (1, 10, 100 mM $NaNO_3$); Experimental conditions: initial Pb concentration, 1 mM: 9.38 mg/L; 10 mM: 9.25 mg/L; 100 mM: 10.06 mg/L

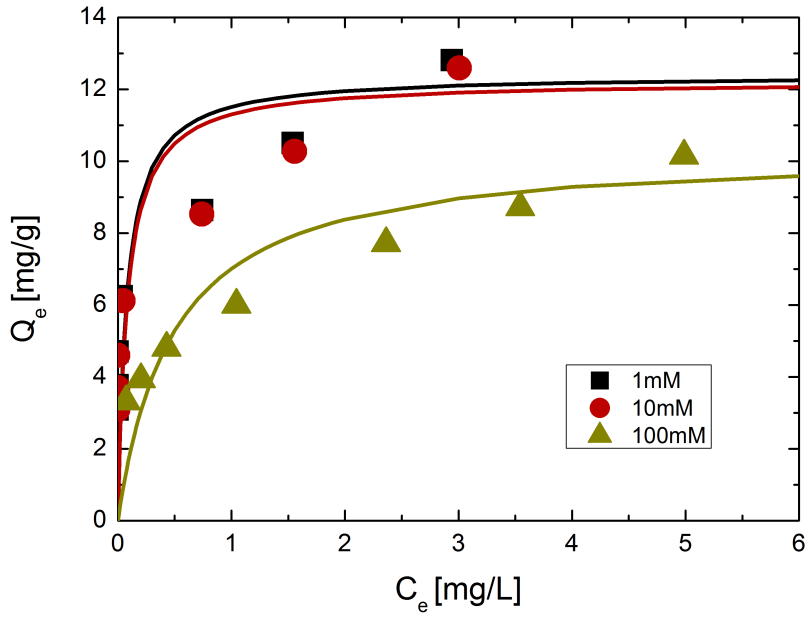

Figure 5.18: Langmuir model fitted to isotherm experiments (Batch 1) of Pb with different ionic strengths (1, 10, 100 mM $NaNO_3$); Experimental conditions: initial Pb concentration, 1 mM: 9.38 mg/L; 10 mM: 9.25 mg/L; 100 mM: 10.06 mg/L

Regarding the experimental data, the adsorption at 1 mM and 10 mM ionic strength are pretty identical so the difference in salt concentration in that range does not make a big difference. The data of the 100 mM experiment differs from the others two and is significantly lower which means that in this range the ionic strength has an impact on the adsorption capacity of lead to hematite.

Of the three models fitted to the experimental data, the Langmuir model has the highest R^2 value shown in table 5.10. To compare the models, the Langmuir model (see figure 5.18) and the Freundlich model (see figure 5.17) were plotted.

The Freundlich model shows a good fit for the 100 mM data which also has the highest R^2 value of 0.975 for this model. Although the other two plots seem to differ slightly from the experimental data, especially in the higher concentration range, they have high R^2 values. This is due to the three points at very low concentration of the lead in the solution when almost all lead is adsorbed. The model fits to that situation pretty well but cannot depict the behavior in higher concentration regions.

The Langmuir model seems to fit better at higher C_e concentration than the Freundlich model whereas the Freundlich model depicts the experimental data better at low concentrations of C_e. For the calculated Q_{max} of the Langmuir model the same tendency can be seen as for the experimental data regarding the influence of the ionic strength. The value for 100 mM is about 16% lower than the value of 1 mM whereas the value of 10 mM only differs less than 2% (see table 5.11).
The parameters for the Temkin model of 1 mM and 10 mM become very high due to the high adsorption.

Table 5.10: R^2 values for the different fitted isotherm models of Pb with different ionic strengths ($NaNO_3$)

Pb Case	Freundlich	Langmuir	Temkin
pH 6, 1 mM	0.926	**0.979**	0.855
pH 6, 10 mM	0.914	**0.981**	0.853
pH 6, 100mM	0.975	**0.976**	0.913

Table 5.11: Parameters for the different fitted isotherm models of Pb with different ionic strengths ($NaNO_3$)

Pb Case	Freundlich		Langmuir		Temkin	
	K_f	n	Q_{max} [mg/g]	b	A_T	b_T [kJ/mol]
pH 6, 1 mM	9.87	8.72	**12.42**	12.58	556199	3.14
pH 6, 10 mM	9.74	8.76	**12.24**	12.01	1107391	3.64
pH 6, 100mM	6.55	3.92	**10.42**	2.06	93.59	1.57

5.3.4 Nickel

The two base cases of nickel at pH 7 are shown in figure 5.19. The pH is almost constant and in both experiments between 6.8 and 7.0. The adsorption of nickel to hematite is slowly increasing over the range of C_e except the last points which jump again and were excluded for the calculation as in all other models. For further investigation there should be done more experiments with a higher hematite concentration or a lower metal concentration to

get a better insight of the whole adsorption range.

The maximum Q_e measured is 2.91 mg/g at a C_e of 9.90 mg/L (the point of 0.1 g/L hematite is excluded).

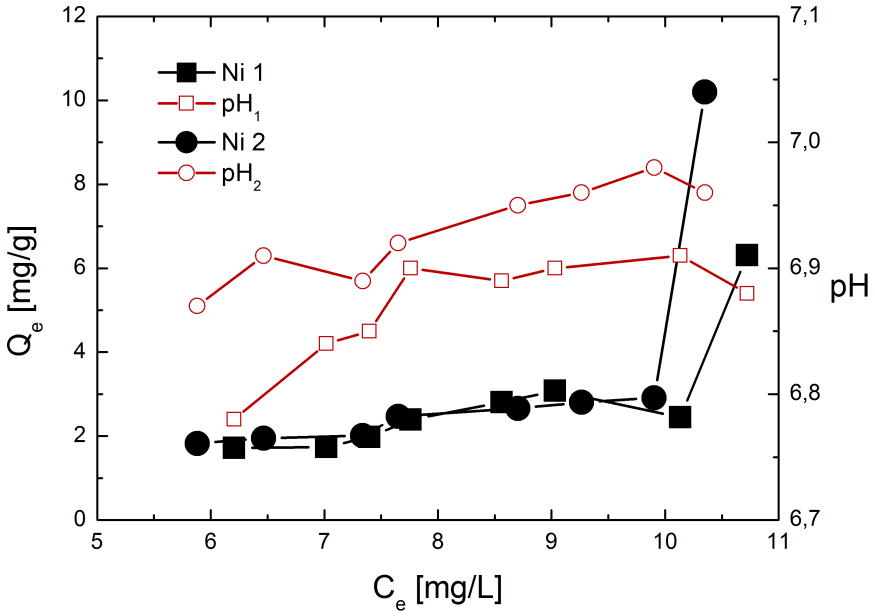

Figure 5.19: Isotherms Ni and pH measured after experiments; experimental conditions: initial Ni concentration, Batch 1: 11.36 mg/L, Batch 2: 10.62 mg/L; pH blank 1: 6.92, pH blank 2: 6.98; 10 mM $NaNO_3$; temperature, $19 \pm 2°C$

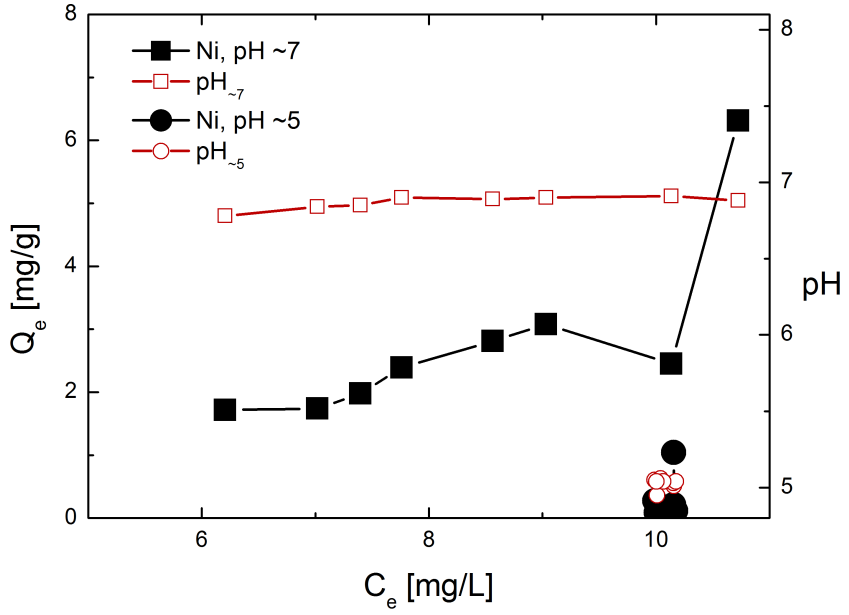

Figure 5.20: Comparison of Isotherms of Ni at pH 5 and 7; experimental conditions: initial Ni concentration, pH 5: 10.16 mg/L, pH 7: 10.62 mg/L; pH of blank, pH 5: 5.02, pH 7: 6.98; 10 mM $NaNO_3$; temperature, $21 \pm 3°C$

In figure 5.20 adsorption at pH 7 and pH 5 is compared. The adsorption at pH 5 is negligible and so there is no isotherm plot to identify. There is only a cloud of points all in the area of the initial concentration of the metal solution. So pH 7 is a better range to adsorb than pH 5 for nickel. This is in compliance with [63] which reports a strong adsorption edge meaning that in a small range of pH the adsorption changes significantly. Figure 4.6 shows this edge for nickel amongst other metals.

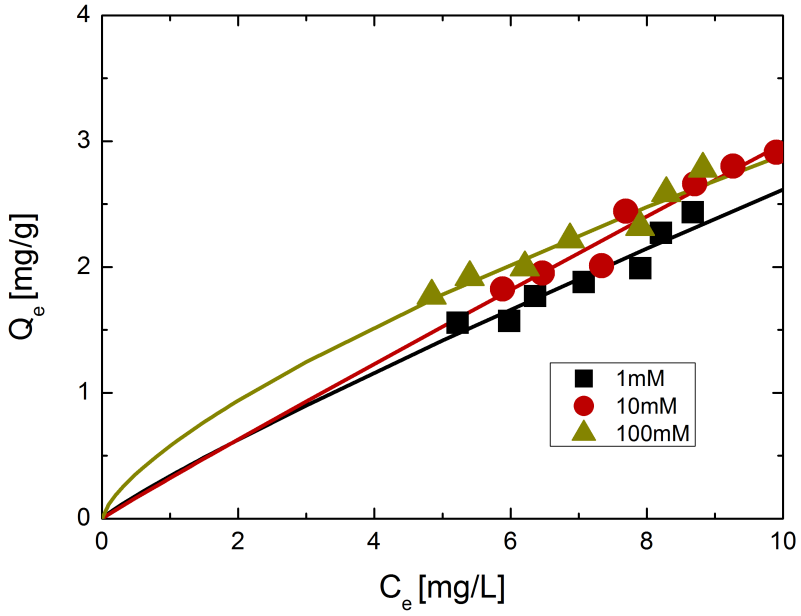

Figure 5.21: Freundlich model fitted to isotherm experiments (Batch 1) of Ni with different ionic strengths (1, 10, 100 mM $NaNO_3$); Experimental conditions: initial Ni concentration, 1 mM: 9.91 mg/L; 10 mM: 11.36 mg/L; 100 mM: 10.21 mg/L

For the nickel adsorption at pH 7 the three models were fitted and compared. The Freundlich models seems to fit the best regarding R^2 values (see table 5.12), although they do not differ much between the models.

In figure 5.21 the Freundlich model is shown. It seems that the influence of ionic strength is weak. Only small difference could be identified. Nickel is slightly less adsorbed with an ionic strength of 1 mM than with 10 mM or 100 mM. However that tendency could change at higher C_e concentrations. Therefore more experimental data should be obtained for the lower and higher C_e range to identify the whole isotherm plot.

In table 5.12 the R^2 values for the Langmuir model are shown. There are listed two values. The difference between those values is the linearization method and the values disagree significantly. This shows that the R^2 values should always be interpreted cautiously knowing that there are more than one possibility to linearize the Langmuir model and it depends which one is chosen (see beginning of this section).

The Langmuir parameters were calculated with the linearization method with higher R_2

values. All calculated parameters are shown in table 5.13 and the Q_{max} parameter differ significantly from the maximum adsorption value measured during the experiments. The slope of the adsorption model indicates that the maximum capacity of nickel adsorbed to hematite is higher than the maximum Q_e measured. However the values of Q_{max} differ so much from what is expected and between each other that it seems that these values are not representing a realistic adsorption model.

Table 5.12: R^2 values for the different fitted isotherm models of Ni with different ionic strengths ($NaNO_3$), *linearization method presented in section 3.2.5

Ni Case	Freundlich	Langmuir	Temkin
pH 7, 1 mM	0.914	0.104/0.905*	0.889
pH 7, 10 mM	0.939	0.013/0.932*	0.938
pH 7, 100mM	0.950	0.714/0.948*	0.924

Table 5.13: Parameters for the different fitted isotherm models of Ni with different ionic strengths ($NaNO_3$)

Ni Case	Freundlich		Langmuir		Temkin	
	K_f	n	Q_{max} [mg/g]	b	A_T	b_T [kJ/mol]
pH 7, 1 mM	0.34	1.13	12.33	0.03	0.44	1,42
pH 7, 10 mM	0.32	1.03	52.08	$6.04 \cdot 10^{-3}$	0.37	1,08
pH 7, 100mM	0.58	1.43	6.74	0.07	0.62	1.56

Comparison with other adsorbents

Other works already tested the adsorption potential for heavy metals to other adsorbents, some even for hematite. However, it is difficult to compare these results easily because a lot of parameter play an important role such as pH, initial concentrations, temperature, adsorption time etc.. To get a better understanding and a possibility to compare, different related articles are mentioned and briefly described. Table 5.14 provides an overview of the capacities of other adsorbents. The values in table 5.14 for the hematite of this work are

chosen to be the calculated Q_{max} from the Langmuir isotherm model except the value for nickel which is the highest measured one not excluded because the Langmuir model was not fitting well enough.

The adsorption potential of biomaterials for chromium(VI) is reviewed in [32], and sorption capacities are compared. It seems like biosorbents can be an efficient way to remove hexavalent chromium but the progress in commercializing these processes is slow.

In [76] magnetite-hematite nanoparticles are investigated to remove metal ions from water, respectively to this study chromium(III) and lead(II). An adsorption capacity of 617.3 mg/g for the Pb(II) and 277 mg/g at pH 7 is reported for the nanomaterial.

Calcite, zeolite, sand and iron filings are examined in order to remove metal ions (Cd, Cu, Pb, Ni, Zn and Cr) from stormwater in [62]. Lead was removed between 95-100% by calcite, zeolite and iron filings, nickel 90% by yeolite and chromium 100% by iron filings. The sand achieved lower percentages. The adsorption processes could be described by the Langmuir or Freundlich isotherm model.

Heavy metal removal from water, including all investigated metals in this work, by nanosized metal oxides is reviewed in[77] and gives a comprehensive overview of different materials and process approaches.

[78] reports efficient chromium(VI) removal by nanoscale maghemite particles which is highly pH dependent and adsorption isotherms can be modeled with the Freundlich equation.

In [79] the sorption of heavy metals to blast furnace sludge is examined and in [80] the same author investigates the adsorbent properties of red mud which contains about 30% hematite. The red mud adsorption was modeled with the Freundlich isotherm model and the blast furnace sludge seems to be following an Langmuir isotherm model for Pb(II) and Cr(III). For adsorption properties, see table 5.14.

Sorption kinetics of different metals including Ni(II) are investigated in [70] onto hematite and report an uptake of nickel after 30 days of 26.5% at pH 6.8 for a system with a concentration of 0.125 mM of Ni(II) which is the equivalent of around 7.3 mg/L. The uptake of the kinetic study in this work at pH 7 of Ni(II) was about 42% which could be higher because of the higher initial concentration or the higher specific surface area.

Table 5.14: Comparison of hematite with other adsorbents

Material	**Capacity [mg/g]**	**pH**	**Reference**
Cr(III)			
Polyvinylalc/sod. alginate	59.9	6	[81]
EDHPA onto Amberlite XAD7	3.0	3	[82]
Hydrous TiO_2	5.0	2	[83]
Activated carbon	19.2	2	[84]
Lignocellulosic waste	285.7	2	[85]
Nano-Fe_3O_4	277.0	7	[76]
Hematite from Ferroxane	12.1	5	This study
Cr(VI)			
Maize bran	312.5	2	[86]
Spent activated clay	0.74-1.42	2	[87]
Nanoscale maghemite	19.2	2-3	[78]
Diatomite	11.6	3	[88]
Anatase	14.6	2.5-5	[89]
Activated carbon (oxidized with nitric acid)	15.5	4-6	[90]
Hematite from Ferroxane	2.9	5	This study
Pb(II)			
Activated Firmiana simplex leaf	379.3	6	[91]
SiO_2/graphene	113.6	6	[92]
Polyampholyte	202.0	6	[93]
PS-EDTA resin	32.1	6	[94]
K. birnessite	164.3	7	[95]
Nano-Fe_3O_4	617.3	7	[76]
Hematite from Ferroxane	12.4	6	This study
Ni(II)			
Red mud	10.9	7.8	[80]
Multi-walled carbon nanotubes	18.1	6	[96]
Carbon nanotubes/iron oxide	9.2	6-7	[97]
Oxidized carbon nanotubes	49.3	6	[96]
Hematite from Ferroxane	2.9	7	This study

5.4 Zeta potential and adsorption mechanism

As a final experiment, the zeta potential of the hematite with and without metals in the water was measured by varying the pH. As described in section 3.2.6, the zeta potential can describe the surface charge, respectively charge at the boundary layer (liquid-slipping plane) of a particle in a liquid which can provide a better understanding of the adsorption mechanism.

In an aqueous medium the Fe-oxide/H_20 interface can acquire a charge by protonation or deprotonation of the neutral sites (-OH groups) as follows:

$$= FeOH \ + \ OH^- \ \rightleftharpoons = Fe(OH)_2{}^- \tag{5.3}$$

The H^+ and OH^- are the potential determining ions and the surface charge at the Fe-oxide/H_20 interface depends on the pH of the solution. Generally, the zero point of charge (ZPC) of an oxide is the pH at which the net surface charge on the oxide surface in an aqueous solution is zero.[98]

The isoelectric point (IEP) of an oxide is the pH at which the oxide particles are electrokinetically uncharged. ZPC and IEP are identical when there is no specific adsorption.[99]

Specific adsorption involves interaction with deprotonated surface hydroxyl groups to form a mono- and bi-nuclear, inner sphere complexes, i.e. for cations (Cr^{+3}, Pb^{+2}, Ni^{+2})

$$\equiv FeOH \ + \ M^{Z+} \ \rightleftharpoons \ \equiv FeOM^{(z-1)^+} \ + \ H^+ \tag{5.4}$$

$$\equiv (FeOH)_2 \ + \ M^{Z+} \ \rightleftharpoons \ \equiv (Fe-O)_2 M^{(z-2)^+} \ + \ H^+ \tag{5.5}$$

whereas for inorganic anions which are ligands such as chromate ($[HCrO_4]^-$), replace the -OH groups, thus forming the inner-sphere surface complexes:

$$\equiv FeOH \ + \ L^- \ \rightleftharpoons \ \equiv FeL \ + \ OH^- \tag{5.6}$$

$$\equiv(FeOH)_2 \; + \; L^- \; \rightleftharpoons \; \equiv Fe_2L^+ \; + \; 2OH^- \tag{5.7}$$

Since in this work only the zeta potential was measured and no further spectroscopic techniques were used like FTIR and EXAFS, the surface species can not be fully characterized.[10] However it provides a basic idea of adsorption mechanisms and allows to make some conclusions.

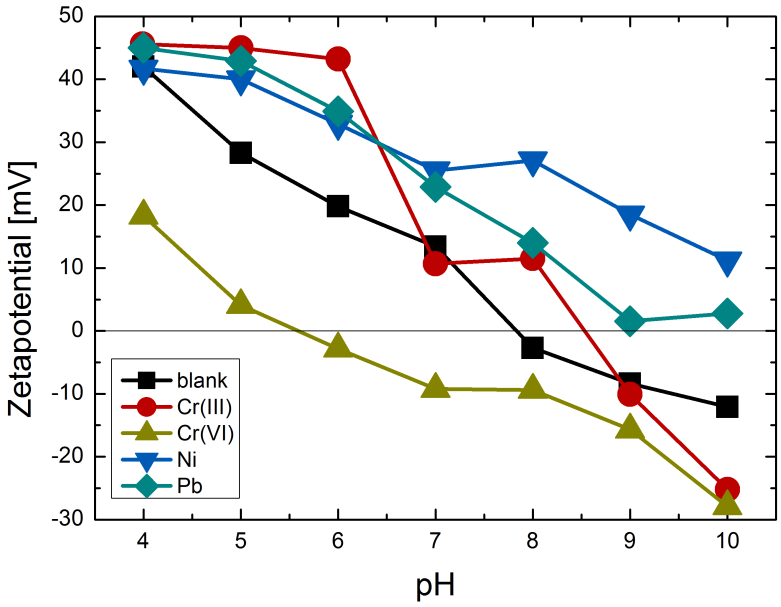

Figure 5.22: Zeta potentials of solutions of different metals depending on pH; experimental conditions: hematite concentration, 1 g/L; initial metal concentrations, 10 mg/L; ionic strength, 10 mM $NaNO_3$; temperature, 20°C; 30 min of mixing before measurement

In figure 5.22 the comparison of hematite in water with only $NaNO_3$ to hematite in water, $NaNO_3$ and one of the investigated metals is shown. The points were obtained by measuring the sample 10 times and taking the median of the results.

The point of zero charge for the base case which is the one without a metal concentration is found to be around a pH of 7.8 which is a little lower to a value found in the literature of 8.5. This difference could be the attributed to the presence of the $NaNO_3$.[100]

Further plots for the solution containing a metal show a rise in the zeta potential except

the hexavalent chromium which shows a decrease. In the observed range of the pH from 4 to 10 the point of zero charge for the solution of trivalent chromium is shifted to about 8.5 whereas the divalent lead and nickel do not even pass the zero. The point of zero charge for the hexavalent chromium is lowered to about pH 5.5.

Thus the isotherm experiment with Cr(VI) at pH 5 was done in an environment with a positive zeta potential and at pH 8 in a negative area of the zeta potential. At pH 8 the adsorbent hardly adsorbed anything whereas at pH 5 it adsorbed about 5 times more. When electrostatics govern adsorption (i.e. nonspecific adsorption), the surface must have an overall positive charge in order for adsorption to take place. In contrast, where specific adsorption is involved an overall positive charge is not required.[10] Therefore it seems that the hexavalent chromium adsorption combines the both mechanisms. but the nonspecific adsorption is dominating or the number of $FeOH_2{}^+$ decreases with a rising pH. Other studies support the theory of the decrease of the $FeOH_2{}^+$ groups and with it the inner sphere complexation.[101]

The adsorption isotherm of the trivalent chromium showed a significant decrease in pH with higher concentration of hematite, thus total amount of chromium adsorbed. This decrease could be due to the release of H^+ during the specific adsorption shown in equation 5.4 and 5.5. At the investigated pH of 5 the calculated ion in the solution, shown in 3.6, is mainly $[CrOH]^{2+}$ which is a cation and would conclude a specific adsorption. Further the zeta potential increased significantly with trivalent chromium in the solution at pH 5.

Likewise, the zeta potential increased with the lead ions in the water at pH 5 and pH 6 as well as with nickel at pH 5 and 7. However the pH stays more or less constant and shows only a slight decrease at high hematite concentrations in the two batches for nickel and one for lead (see figure 5.20 and 5.16). In [63], hematite is reported to be a good adsorbent for lead and as well has a maximum at around pH 6. Nickel, however, is less adsorbed and has a maximum at around pH 7. This is in compliance with this work.

5.5 Process design possibilities

To include the investigated material in a working process, some approaches have been undertaken and will be presented in the following section. Before developing a solution, the first thing is to define the purpose of the product and the demands to it. The purpose for this product in Argentina is a filter system for households or smaller schools, so rather small to medium scales.
So in this case, the system should be

- easy to use.
- easy to install.
- affordable to buy
- economic to maintain.

In general, the process possibilities can be divided into two big groups. One approach is to aggregate the particles in a way and use it in a bulk filter or a process which filters the particles at the end. The other approach is to fix the particles in a certain way on another material or structure which then is used in the aimed process.[102–105]
Several supports have been investigated by other authors include natural hosts such as bentonite [106, 107], sand [108, 109], and montmorillonite [110], metallic oxide materials such as Al_2O_3 membrane [111] and porous manganese oxide complex [112], and synthetic polymer hosts such as cross-linked ion-exchange resins.[113–115]

Membranes

Former works at Instituto Technologico de Buenos Aires (ITBA), Argentina tried to use a porous alumina tube and embedded and attached the Ferroxane to it. Subsequently the ceramic membrane was sintered which converted the Ferroxane particles on and in the membrane to hematite. In figure 5.23, these coated membranes are shown. These tubes could be used in a dead end setup to filter the contaminated water. In the experiments, the treated membranes were used to filter arsenic which proved to work. The membrane works with a low transmembrane pressure drop and so no pumping is necessary. One challenge of the process is, how to attach a satisfying amount of hematite to the porous alumina

tube. Considering the costs for the membrane, the alumina tube is the most expensive part. However, those tubes are expected to withstand various regeneration cycles which cut costs of the total process. In addition to this, ferroxane-derived ceramic membranes have removal capabilities in the ultrafiltration range, being effective for the separation of organic macromolecules, inorganic colloidal particles and bacteria. [12, 13, 116]

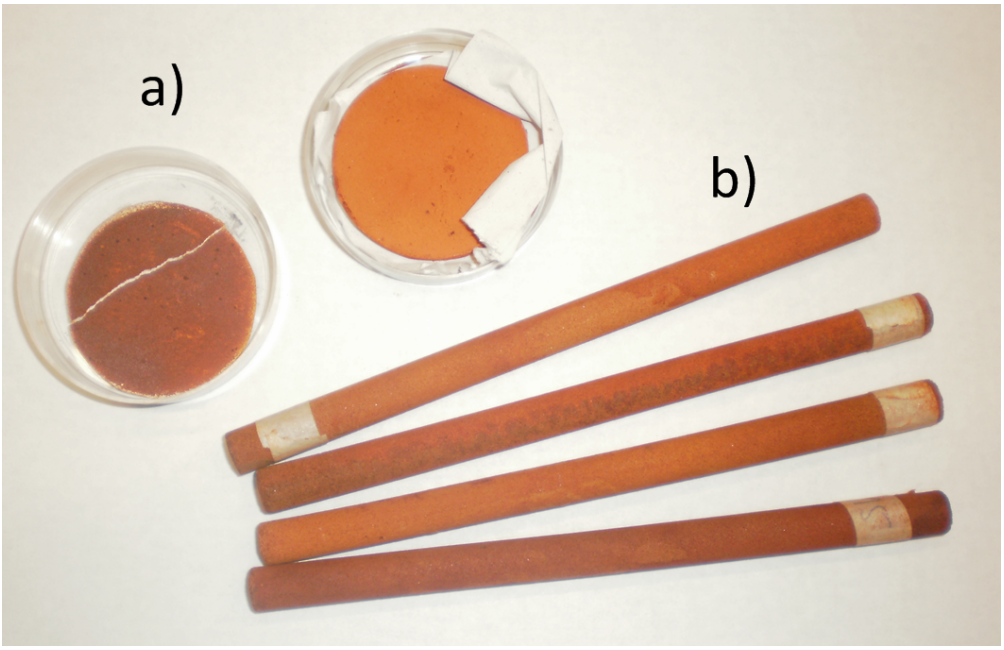

Figure 5.23: Different design possibilities: a) Pellet made out of hematite (after burning on the left) and ferroxane (before burning on the right) b) Porous alumina tube embedded and coated with hematite

Pellets

Another approach done at Instituto Technologico de Buenos Aires (ITBA), Argentina is synthesizing pellets made out of aluminum oxide. The aluminum oxide was mixed with the ferroxane and the burned in an oven. Figure 5.23 shows these pellets in a) before and after the burning procedure. So far, there need to be done more research on how getting a stable pellet that has optimal adsorption properties.

The idea is to design a device that uses the pellets to filter the water and which can be changed quickly and easily.

Bulk filter

Bulk filter like adsorption columns always have a trade off between particle size, surface area respectively and pressure drop over the column. Therefore a tunable material of which the particle size can be adjusted to the conditions is important. Several works and also commercial products have been developed in this area.

GEH® Wasserchemie developed a granular ferric hydroxide for heavy metal removal. It is a mix of $\beta - FeOOH$ and $Fe(OH)_3$. It adsorbs heavy metals such as chromium, uranium, copper and lead as well as toxic elements icluding arsenic, antimony, vanadium and selenium. The particle size is between 0.2-2 mm and has a surface area of around $300m^2/g$.[117]

To granulate the particles a process is used which is similar to freeze-thaw conditioning presented in [118]. It uses high pressures and low temperatures. That process is patented [119] by that company.[120]

There is another work [121] which experimented with sand coated with iron oxides to get a filtration material for developing countries like Nepal which presents several different methods to synthesize these coated sands. This could be a cheap way to get a acceptable bulk size for filter.

In [122], magnetite is embedded in Zeolithes to produce a magnetic adsorbent. Zeolithes show good adsorption properties and a huge surface area (around $500m^2/g$) and the magnetite leads to a magnetic composite which can be used in an adsorption process and be separated by a magnetic process. Hematite has no magnetic properties but the combination of two materials to a composite often enhances certain properties.

Kolshi filter

For developing countries like Nepal, Bangladesh and other south-asian countries, some ferric oxide filter system have been developed, mainly for arsenic removal. The filters normally use the effect of rust on iron filing by putting it into contact with water. Then the water passes these iron filings and continue to a sand layer before leaving the system. Most of these filters are very basic and try to provide clean drinking water for family homes with no direct connection to drinking water.

One of the simplest solution called Kolshi filter is shown in figure 5.24. The water passes each one of the containers. The first tank is the raw water from which the water goes into the container with the iron filings to adsorb the heavy metal, respectively arsenic. The next tank contains sand to trap the particles and with it the adsorbed metal and the last one collects the clean water.[123]

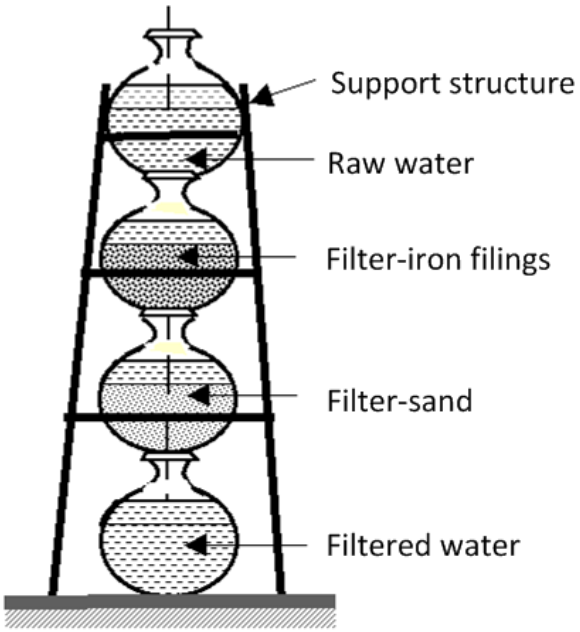

Figure 5.24: Kolshi filter

6 Conclusion and future work

The objective of this work was to investigate the ability of hematite to adsorb heavy metals, more precisely trivalent and hexavalent chromium, nickel and lead. As a final step, possible ways to integrate the material in process were presented.
The procedure was divided into three phases:

- Synthesis and characterization of the used material
- Investigation of adsorption by obtaining kinetics and isotherms
- Identifying process possibilities

In the first step hematite was prepared by a reaction in three steps. First lepidocrocite was synthesized which then was coated with acetic acid to get ferroxane. Finally the ferroxane was burned to obtain the used hematite. Analysis was done regarding surface area, composition and particle size. The hematite had a specific surface area (BET) of 37.54 m^2/g and an average particle size of 337 nm.
All obtained adsorption kinetics showed a satisfying state of equilibrium after 48 hours and so the adsorption isotherm experiments were conducted in that time frame. All metals showed a very good compliance with the pseudo-second-order kinetic model.
The adsorption isotherms were investigated at two different pH per metal except Cr(III) and three different ionic strengths (1 mM, 10 mM, 100 mM). The maximum amount of Cr(III) adsorbed to hematite was 10.52 mg/g at pH 5 and the amount of salt had a significant lowering influence on the adsorption with higher concentrations. However Cr(VI) showed no effect by changing the ionic strength but the maximum value adsorbed was lower with 2.88 mg/g at pH 5. Pb was adsorbed best with a maximum value of 12.24 mg/g at pH 6 and ionic strength seems to have a lowering influence on adsorption only at high concentrations (100mM). The adsorption of Ni showed a maximum value of 2.9 mg/g at pH 7 but the

isotherm indicated to have more potential regarding the maximum load.
The Freundlich isotherm model showed best compliance for Cr(III) and Ni(II) whereas Cr(VI) and Pb(II) exhibited Langmuir model behavior. However the work also showed how linearizations can change compliances regarding R^2 values.
As a last step, possible process steps are presented regarding the idea of designing a filtration technology to use in household or small-scale application.

Outlook and Future work

Hematite could be identified as a good adsorbent for Cr(III) and Pb in this work and showed promising adsorption properties for arsenic in former works. The cost of the adsorbent is the big advantage for a usage in small-scale applications in rural areas.[12, 13] A further investigation of Ni adsorption isotherms should be conducted and a broader range of pH should be tested for all metals.
The key issue that should be addressed now is the design and prototype of a process. Various ideas were shown and the most promising seem to be a combination of two materials. That compound could exhibit greater adsorption properties than the single materials and can be integrated as a bulk filter with a zeolithe, sand or other high-specific surface material or as a coated membrane with additional ultrafiltration properties. With an existing prototype a continuous filtration could be tested and breakthrough curves could be obtained in case of a bulk filter.

7 Bibliography

[1] M. Qasim M. Jamil, M.S. Zia. Contamination of agro−ecosystem and human health hazards from wastewater used for irrigation. *J.Chem. Soc.Pak.*, 32:370−−378, 2010.

[2] Jin-Song Hu, Liang-Shu Zhong, Wei-Guo Song, and Li-Jun Wan. Synthesis of hierarchically structured metal oxides and their application in heavy metal ion removal. *Advanced Materials*, 20(15):2977–2982, 2008.

[3] Quality of Water for Human Consumption: The Health of the Population Residing in the Matanza-Riachuelo River Basin Area in Greater Buenos Aires. *Salud Colectiva 9.1*, 9.1:53–63, 2013.

[4] Evaluating, monitoring small scale gold mining, mercury use: Building a knowledge-base with satellite imagery, and field work. *UNIDO*, 2007.

[5] Fenglian Fu and Qi Wang. Removal of heavy metal ions from wastewaters: A review. *Journal of Environmental Management*, 92:407 – 418, 2011.

[6] Yuen-Hua Wang, Su-Hsia Lin, and Ruey-Shin Juang. Removal of heavy metal ions from aqueous solutions using various low-cost adsorbents. *Journal of Hazardous Materials*, 102:291 – 302, 2003.

[7] David William O Connell, Colin Birkinshaw, and Thomas Francis O Dwyer. Heavy metal adsorbents prepared from the modification of cellulose: A review. *Bioresource Technology*, 99(15):6709–6724, 2008.

[8] Tonni Agustiono Kurniawan, Gilbert Y.S. Chan, Wai-Hung Lo, and Sandhya Babel. Physico-chemical treatment techniques for wastewater laden with heavy metals. *Chemical Engineering Journal*, 118:83–98, 2006.

[9] N Galil and M Rebhun. Primary chemical treatment minimizing dependence on bio-process in small treatment plants. *Water Science & Technology*, 22:203–210, 1990.

[10] R.M. Cornell and U.Schwertmann. *The Iron Oxides*. Wiley-VCH, 2006.

[11] Jerome Rose, Maria M. Cortalezzi-Fidalgo, Stephane Moustier, Cyrille Magnetto, Christopher D. Jones, Andrew R. Barron, Mark R. Wiesner, and Jean-Yves Bottero. Synthesis and characterization of carboxylate-feooh nanoparticles (ferroxanes) and ferroxane-derived ceramics. *Chemistry of Materials*, 14(2):621–628, 2002.

[12] P. Sabbatini, F. Rossi, G. Thern, A. Marajofsky, and M.M. Fidalgo de Cortalezzi. Iron oxide adsorbers for arsenic removal: A low cost treatment for rural areas and mobile applications. *Desalination*, 248:184 – 192, 2009.

[13] P. Sabbatini, F. Yrazu, F. Rossi, G. Thern, A. Marajofsky, and M.M. Fidalgo de Cortalezzi. Fabrication and characterization of iron oxide ceramic membranes for arsenic removal. *Water Research*, 44(19):5702 – 5712, 2010. Groundwater Arsenic: From Genesis to Sustainable Remediation.

[14] Pradyot Patnaik. *Handbook of inorganic chemicals*. McGraw-Hill New Yor, 2003.

[15] David Eugene Kimbrough, Yoram Cohen, Arthur M. Winer, Lynn Creelman, and Clayton Mabuni. A critical assessment of chromium in the environment. *Critical Reviews in Environmental Science and Technology*, 29(1):1–46, 1999.

[16] World Health Organization. Chromium in drinking-water. *Guidelines for Drinking-water Quality*, 2003.

[17] World Health Organization. Guidelines for drinking-water quality. *WHO Library Cataloguing*, 4th ed., 2011.

[18] Domy C. Adriano. *Trace Elements in Terrestrial Environments - Biogeochemistry, Bioavailability, and Risks of Metals*. Springer, 2001.

[19] Ministerio de Economía y Finanzas Públicas. Convenios ley 26.221. *Argentinian Law*, 2007.

[20] Y. Schirnding S. Tong and T. Prapamontol. Environmental lead exposure: a public health problem of global dimensions. *Bulletin of the World Health Organization*, 78(9), 2000.

[21] World Health Organization. Nickel in drinking-water. *Guidelines for Drinking-water Quality*, 2005.

[22] Francoise C. Richard and Alain C.M. Bourg. Aqueous geochemistry of chromium: A review. *Water Research*, 25(7):807 – 816, 1991.

[23] J. Kotas and Z. Stasicka. Chromium occurrence in the environment and methods of its speciation. *Environmental Pollution*, 107(3):263 – 283, 2000.

[24] World Health Organization. Guidelines for drinking-water quality health criteria and other supporting information. 2nd ed. Vol. 2., 1996.

[25] Michael Sperling, Shukun Xu, and Bernhard Welz. Determination of chromium(iii) and chromium(vi) in water using flow injection on-line preconcentration with selective adsorption on activated alumina and flame atomic absorption spectrometric detection. *Analytical Chemistry*, 64(24):3101–3108, 1992.

[26] J. L. Pauley and M. K. Testerman. Basic salts of lead nitrate formed in aqueous media1. *Journal of the American Chemical Society*, 76(16):4220–4222, 1954.

[27] Heike B Bradl. Adsorption of heavy metal ions on soils and soils constituents. *Journal of Colloid and Interface Science*, 277(1):1 – 18, 2004.

[28] U. Förstner and G. T. W. Wittmann. *Metal Pollution in the Aquatic Environment*. Springer, 1981.

[29] E. Denkhaus and K. Salnikow. Nickel essentiality, toxicity, and carcinogenicity. *Critical Reviews in Oncology/Hematology*, 42(1):35 – 56, 2002.

[30] K. Sing J. Rouquerol, F. Rouquerol. *Adsorption by Powders and Porous Solids*. Academic Press, 1998.

[31] Kenneth SW Sing. Reporting physisorption data for gas/solid systems with special reference to the determination of surface area and porosity (recommendations 1984). *Pure and applied chemistry*, 57(4):603–619, 1985.

[32] Bidyut Saha and Chris Orvig. Biosorbents for hexavalent chromium elimination from industrial and municipal effluents. *Coordination Chemistry Reviews*, 254:2959 – 2972, 2010.

[33] S. Lagergren. Zur theorie der sogenannten adsorption gelöster stoffe. *Kungliga Svenska Vetenskapsakademiens. Handlingar*, 24 (4):1–39, 1898.

[34] Ho Yuh-Shan. Citation review of lagergren kinetic rate equation on adsorption reactions. *Scientometrics*, 59(1):171–177, 2004.

[35] Y.S Ho and G McKay. Pseudo-second order model for sorption processes. *Process Biochemistry*, 34(5):451 – 465, 1999.

[36] G. Tammann and W. Köster. Metallographische mitteilungen aus dem institut für physikalische chemie der universität göttingen. cv. die geschwindigkeit der einwirkung von sauerstoff, schwefelwasserstoff und halogenen auf metalle. *Zeitschrift für anorganische und allgemeine Chemie*, 123(1):196–224, 1922.

[37] C. Aharoni and F.C. Tompkins. Kinetics of adsorption and desorption and the elovich equation. volume 21 of *Advances in Catalysis*, pages 1 – 49. Academic Press, 1970.

[38] Feng-Chin Wu, Ru-Ling Tseng, and Ruey-Shin Juang. Characteristics of elovich equation used for the analysis of adsorption kinetics in dye-chitosan systems. *Chemical Engineering Journal*, 150:366 – 373, 2009.

[39] Y.S. Ho and G. McKay. A comparison of chemisorption kinetic models applied to pollutant removal on various sorbents. *Process Safety and Environmental Protection*, 76(4):332 – 340, 1998.

[40] R. Rajagopalan P.C. Hiemenz. *Principles of Colloid and Surface Chemistry.* Marcel Dekker, Inc., 1997.

[41] RA Pierotti and J Rouquerol. Reporting physisorption data for gas/solid systems with special reference to the determination of surface area and porosity. *Pure Appl Chem*, 57(4):603–619, 1985.

[42] Shields J.E. Thomas M.A. Thommes M. Lowell, S. *Characterization of Porous Solids and Powders: Surface Area, Pore Size and Density.* Kluwer Academic Publishers, 2004.

[43] Irving Langmuir. The adsorption of gases on plane surfaces of glass, mica and platinum. *Journal of the American Chemical Society*, 40(9):1361–1403, 1918.

[44] K.Y. Foo and B.H. Hameed. Insights into the modeling of adsorption isotherm systems. *Chemical Engineering Journal*, 156(1):2 – 10, 2010.

[45] H. Freundlich. Over the adsorption in solution,. *Z. Phys. Chem. 57*, page 385, 1906.

[46] Y.S. Ho, J.F. Porter, and G. McKay. Equilibrium isotherm studies for the sorption of divalent metal ions onto peat: Copper, nickel and lead single component systems. *Water, Air, and Soil Pollution*, 141(1-4):1–33, 2002.

[47] V. Pyzhev M.I. Temkin. Kinetics of ammonia synthesis on promoted iron catalyst. *Acta Phys. Chim. USSR 12*, pages 327–356, 1940.

[48] Malvern Instruments Ltd. *Zetasizer Nano Series User Manual*, 2004.

[49] Russell J. Crawford, Ian H. Harding, and David E. Mainwaring. The zeta potential of iron and chromium hydrous oxides during adsorption and coprecipitation of aqueous heavy metals. *Journal of Colloid and Interface Science*, 181(2):561 – 570, 1996.

[50] G. Kirchhoff and R. Bunsen. Xlii. chemical analysis by spectrum-observations. *Philosophical Magazine Series 4*, 22(148):329–349, 1861.

[51] A. Walsh. The application of atomic absorption spectra to chemical analysis. *Spectrochimica Acta*, 7(0):108 – 117, 1955.

[52] B.V. L'vov. Fifty years of atomic absorption spectrometry. *Journal of Analytical Chemistry*, 60(4):382–392, 2005.

[53] B.V. L'vov. The analytical use of atomic absorption spectra. *Spectrochimica Acta*, 17(7):761 – 770, 1961.

[54] Jose A. C. Broekaert. *Basic Principles*. Wiley-VCH Verlag GmbH & Co. KGaA, 2006.

[55] Stephen Brunauer, P. H. Emmett, and Edward Teller. Adsorption of gases in multimolecular layers. *Journal of the American Chemical Society*, 60(2):309–319, 1938.

[56] Elliott P. Barrett, Leslie G. Joyner, and Paul P. Halenda. The determination of pore volume and area distributions in porous substances. i. computations from nitrogen isotherms. *Journal of the American Chemical Society*, 73(1):373–380, 1951.

[57] George Halsey. Physical adsorption on non-uniform surfaces. *The Journal of Chemical Physics*, 16(10):931–937, 1948.

[58] Claus Urban and Peter Schurtenberger. Characterization of turbid colloidal suspensions using light scattering techniques combined with cross-correlation methods. *Journal of Colloid and Interface Science*, 207(1):150 – 158, 1998.

[59] Yen-Hua Chen and Fu-An Li. Kinetic study on removal of copper(ii) using goethite and hematite nano-photocatalysts. *Journal of Colloid and Interface Science*, 347(2):277 – 281, 2010.

[60] Michel Hoenig and Anne-Marie de Kersabiec. Sample preparation steps for analysis by atomic spectroscopy methods: present status. *Spectrochimica Acta Part B: Atomic Spectroscopy*, 51(11):1297 – 1307, 1996.

[61] United States Environmental Protection Agency (USEPA). United states environmental protection agency (usepa), test methods for evaluating solid waste, physical/chemical methods. Washington, DC, 2007.

[62] Krishna R. Reddy, Tao Xie, and Sara Dastgheibi. Removal of heavy metals from urban stormwater runoff using different filter materials. *Journal of Environmental Chemical Engineering*, 2(1):282 – 292, 2014.

[63] McKenzie RM. The adsorption of lead and other heavy metals on oxides of manganese and iron. *Australian Journal of Soil Research 18*, pages 61–73, 1980.

[64] *COULTER SA 3100 Series Surface Area and Pore Size Analyzers Manual.*

[65] Murat Erdemoglu and Musa Sarikaya. Effects of heavy metals and oxalate on the zeta potential of magnetite. *Journal of Colloid and Interface Science*, 300(2):795 – 804, 2006.

[66] U. Schwertmann J. Torrent and V. Barron. Phosphate sorption by natural hematites. *Eur. J. Soil Sci.*, 45:45–51, 1994.

[67] J. Torrent and U. Schwertmann. Influence of hematite on the color of red beds. *J. Sediment Petrology*, 57:682–686, 1987.

[68] T. Sugimoto and Y. Wang. Mechanism of the shape and structural control of monodispersed $\alpha - fe_2o_3$ particles by sulfate ions. *J. Coll. Interfac. Sci.*, 207:137–149, 1998.

[69] Camden R. Hubbard. Standard x-ray diffraction powder patterns. *National Bureau of Standards*, 1981.

[70] Byong-Hun Jeon, Brian A. Dempsey, William D. Burgos, and Richard A. Royer. Sorption kinetics of fe(ii), zn(ii), co(ii), ni(ii), cd(ii), and fe(ii)/me(ii) onto hematite. *Water Research*, 37(17):4135 – 4142, 2003.

[71] Byong-Hun Jeon, Brian A. Dempsey, William D. Burgos, Richard A. Royer, and Eric E. Roden. Modeling the sorption kinetics of divalent metal ions to hematite. *Water Research*, 38(10):2499 – 2504, 2004.

[72] G. W. Bruemmer, J. Gerth, and K. G. Tiller. Reaction kinetics of the adsorption and desorption of nickel, zinc and cadmium by goethite. i. adsorption and diffusion of metals. *Journal of Soil Science*, 39(1):37–52, 1988.

[73] Yuh-Shan Ho. Selection of optimum sorption isotherm. *Carbon 42*, pages 2115–2117, 2004.

[74] David G. Kinniburgh. General purpose adsorption isotherms. *Environmental Science & Technology*, 20(9):895–904, 1986. PMID: 22263822.

[75] M.Ristic S. Music and M. Tonkovic. Sorption of chromium(vi) on hydrous iron oxides. *Wasser-Abwasser-Forsch.*, 19:186–196, 1986.

[76] M.A. Ahmed, S.M. Ali, S.I. El-Dek, and A. Galal. Magnetite-hematite nanoparticles prepared by green methods for heavy metal ions removal from water. *Materials Science and Engineering: B*, 178(10):744 – 751, 2013.

[77] Ming Hua, Shujuan Zhang, Bingcai Pan, Weiming Zhang, Lu Lv, and Quanxing Zhang. Heavy metal removal from water/wastewater by nanosized metal oxides: A review. *Journal of Hazardous Materials*, 211-212(0):317 – 331, 2012. Nanotechnologies for the Treatment of Water, Air and Soil.

[78] Jing Hu, Guohua Chen, and Irene M.C. Lo. Removal and recovery of cr(vi) from wastewater by maghemite nanoparticles. *Water Research*, 39(18):4528 – 4536, 2005.

[79] A. Lopez-Delgado, C. Perez, and F.A. Lopez. Sorption of heavy metals on blast furnace sludge. *Water Research*, 32(4):989 – 996, 1998.

[80] E. Lopez, B. Soto, M. Arias, A. Nunez, D. Rubinos, and M.T. Barral. Adsorbent properties of red mud and its use for wastewater treatment. *Water Research*, 32:1314 – 1322, 1998.

[81] Jian Hua Chen, Guo Ping Li, Qing Lin Liu, Jian Cong Ni, Wen Bing Wu, and Jin Mei Lin. Cr(iii) ionic imprinted polyvinyl alcohol/sodium alginate (pva/sa) porous composite membranes for selective adsorption of cr(iii) ions. *Chemical Engineering Journal*, 165:465 – 473, 2010.

[82] M. Ciopec, C.M. Davidescu, A. Negrea, I. Grozav, L. Lupa, P. Negrea, and A. Popa. Adsorption studies of cr(iii) ions from aqueous solutions by dehpa impregnated onto amberlite xad7- factorial design analysis. *Chemical Engineering Research and Design*, 90(10):1660 – 1670, 2012.

[83] H Tel, Y Altay, and M.S Taner. Adsorption characteristics and separation of cr(iii) and cr(vi) on hydrous titanium(iv) oxide. *Journal of Hazardous Materials*, 112:225–231, 2004.

[84] J. Rivera-Utrilla and M. Sanchez-Polo. Adsorption of cr(iii) on ozonised activated carbon. importance of cπ-cation interactions. *Water Research*, 37(14):3335 – 3340, 2003.

[85] K.K. Singh, R. Rastogi, and S.H. Hasan. Removal of cr(vi) from wastewater using rice bran. *Journal of Colloid and Interface Science*, 290(1):61 – 68, 2005.

[86] S.H. Hasan, K.K. Singh, O. Prakash, M. Talat, and Y.S. Ho. Removal of cr(vi) from aqueous solutions using agricultural waste (maize bran). *Journal of Hazardous Materials*, 152:356–365, 2008.

[87] Chih-Huang Weng, Y.C. Sharma, and Sue-Hua Chu. Adsorption of cr(vi) from aqueous solutions by spent activated clay. *Journal of Hazardous Materials*, 155:65–75, 2008.

[88] T.N. De Castro Dantas, A.A.Dantas Neto, and M.C.P. De A. Moura. Removal of chromium from aqueous solutions by diatomite treated with microemulsion. *Water Research*, 35:2219–2224, 2001.

[89] C.H. Weng, J.H. Wang, and C.P. Huang. Adsorption of cr(vi) onto tio2 from dilute aqueous solutions. *Water Science and Technology*, 35(7):55–62, 1997. Adsorption in the Water Environment and Treatment Processes Selected Proceedings of the 1st International Specialized Conference on Adsorption in the Water Environment and Treatment Processes.

[90] Sandhya Babel and Tonni Agustiono Kurniawan. Cr(vi) removal from synthetic wastewater using coconut shell charcoal and commercial activated carbon modified with oxidizing agents and/or chitosan. *Chemosphere*, 54(7):951–967, 2004.

[91] Zhenze Li, Xiaowu Tang, Yunmin Chen, Liming Wei, and Yan Wang. Activation of firmiana simplex leaf and the enhanced pb(ii) adsorption performance: Equilibrium and kinetic studies. *Journal of Hazardous Materials*, 169:386 – 394, 2009.

[92] Liying Hao, Hongjie Song, Lichun Zhang, Xiangyu Wan, Yurong Tang, and Yi Lv. Sio2/graphene composite for highly selective adsorption of pb(ii) ion. *Journal of Colloid and Interface Science*, 369(1):381 – 387, 2012.

[93] Guillermo J. Copello, Luis E. Diaz, and Viviana Campo Dall Orto. Adsorption of cd(ii) and pb(ii) onto a one step-synthesized polyampholyte: Kinetics and equilibrium studies. *Journal of Hazardous Materials*, 217-218(0):374 – 381, 2012.

[94] Liyuan Wang, Liuqing Yang, Yanfeng Li, Yun Zhang, Xiaojie Ma, and Zhengfang Ye. Study on adsorption mechanism of pb(ii) and cu(ii) in aqueous solution using ps-edta resin. *Chemical Engineering Journal*, 163(3):364 – 372, 2010.

[95] E. Eren, H. Gumus, and A. Sarihan. Synthesis, structural characterization and pb(ii) adsorption behavior of k- and h-birnessite samples. *Desalination*, 279:75 – 85, 2011.

[96] Munther Issa Kandah and Jean-Luc Meunier. Removal of nickel ions from water by multi-walled carbon nanotubes. *Journal of Hazardous Materials*, 146:283–288, 2007.

[97] Changlun Chen, Jun Hu, Dadong Shao, Jiaxing Li, and Xiangke Wang. Adsorption behavior of multiwall carbon nanotube/iron oxide magnetic composites for ni(ii) and sr(ii). *Journal of Hazardous Materials*, 164:923–928, 2009.

[98] G. A. Parks and P. L. de Bruyn. The zero point of charge of oxides. *The Journal of Physical Chemistry*, 66(6):967–973, 1962.

[99] S. Music and M. Ristic. Adsorption of trace elements or radionuclides on hydrous iron oxides. *Journal of Radioanalytical and Nuclear Chemistry*, 120(2):289–304, 1988.

[100] A Breeuwsma and J Lyklema. Physical and chemical adsorption of ions in the electrical double layer on hematite ($\alpha - fe_2o_3$). *Journal of Colloid and Interface Science*, 43:437 – 448, 1973. Kendall Award Symposium 163rd American Chemical Society Meeting.

[101] Scott Fendorf, Matthew J. Eick, Paul Grossl, and Donald L. Sparks. Arsenate and chromate retention mechanisms on goethite. 1. surface structure. *Environmental Science & Technology*, 31(2):315–320, 1997.

[102] Min Jang, Weifang Chen, and Fred S. Cannon. Preloading hydrous ferric oxide into granular activated carbon for arsenic removal. *Environmental Science & Technology*, 42(9):3369–3374, 2008. PMID: 18522120.

[103] Kai Loon Chen, Steven E. Mylon, and Menachem Elimelech. Enhanced aggregation of alginate-coated iron oxide (hematite) nanoparticles in the presence of calcium, strontium, and barium cations. *Langmuir*, 23(11):5920–5928, 2007. PMID: 17469860.

[104] Birgitte A. Hansen, Pierre Kwan, Mark M. Benjamin, Chi-Wang Li, and Gregory V. Korshin. Use of iron oxide-coated sand to remove strontium from simulated hanford tank wastes. *Environmental Science & Technology*, 35(24):4905–4909, 2001. PMID: 11775169.

[105] J.M. Zachara, S.C. Smith, and L.S. Kuzel. Adsorption and dissociation of co-edta complexes in iron oxide-containing subsurface sands. *Geochimica et Cosmochimica Acta*, 59(23):4825 – 4844, 1995.

[106] Erdal Eren. Removal of lead ions by unye (turkey) bentonite in iron and magnesium oxide-coated forms. *Journal of Hazardous Materials*, 165:63 – 70, 2009.

[107] E. Eren, A. Tabak, and B. Eren. Performance of magnesium oxide-coated bentonite in removal process of copper ions from aqueous solution. *Desalination*, 257:163 – 169, 2010.

[108] Po-Yu Hu, Yung-Hsu Hsieh, Jen-Ching Chen, and Chen-Yu Chang. Characteristics of manganese-coated sand using sem and edax analysis. *Journal of Colloid and Interface Science*, 272(2):308 – 313, 2004.

[109] Seung-Mok Lee, Won-Gee Kim, C. Laldawngliana, and Diwakar Tiwari. Removal behavior of surface modified sand for cd(ii) and cr(vi) from aqueous solutions. *Journal of Chemical Engineering*, 55(9):3089–3094, 2010.

[110] Ming Fan, Thipnakarin Boonfueng, Ying Xu, Lisa Axe, and Trevor A. Tyson. Modeling pb sorption to microporous amorphous oxides as discrete particles and coatings. *Journal of Colloid and Interface Science*, 281(1):39 – 48, 2005.

[111] Shuna Zhang, Fangyi Cheng, Zhanliang Tao, Feng Gao, and Jun Chen. Removal of nickel ions from wastewater by $mg(oh)_2/mgo$ nanostructures embedded in al_2o_3 membranes. *Journal of Alloys and Compounds*, 426:281 – 285, 2006.

[112] Junichi Otsu and Yoshito Oshima. New approaches to the preparation of metal or metal oxide particles on the surface of porous materials using supercritical water: Development of supercritical water impregnation method. *The Journal of Supercritical Fluids*, 33(1):61 – 67, 2005.

[113] Bingjun Pan, Hui Qiu, Bingcai Pan, Guangze Nie, Lili Xiao, Lu Lv, Weiming Zhang, Quanxing Zhang, and Shourong Zheng. Highly efficient removal of heavy metals by polymer-supported nanosized hydrated fe(iii) oxides: Behavior and xps study. *Water Research*, 44:815 – 824, 2010.

[114] Qing Su, Bingcai Pan, Bingjun Pan, Qingrui Zhang, Weiming Zhang, Lu Lv, Xiaoshu Wang, Jun Wu, and Quanxing Zhang. Fabrication of polymer-supported nanosized hydrous manganese dioxide (hmo) for enhanced lead removal from waters. *Science of The Total Environment*, 407(21):5471 – 5477, 2009.

[115] Shunli Wan, Xin Zhao, Lu Lv, Qing Su, Huining Gu, Bingcai Pan, Weiming Zhang, Zhengwei Lin, and Jingfei Luan. Selective adsorption of cd(ii) and zn(ii) ions by nano-

hydrous manganese dioxide (hmo)-encapsulated cation exchanger. *Industrial & Engineering Chemistry Research*, 49(16):7574–7579, 2010.

[116] G.F. Wells J.-Y. Bottero A.R. Barron M.M. Cortalezzi, J. Rose and M.R. Wiesner. Ceramic membranes derived from ferroxane nanoparticles: a new route for the fabrication of iron oxide ultrafiltration membranes. *Journal of Membrane Science*, 227:207 – 217, 2003.

[117] GEH(2014). Product data sheet geh 102, homepage of geh wasserchemie gmbh & co. kg, osnabrück, http://www.gehwasserchemie.de.

[118] Annette Hofmann, Manuel Pelletier, Laurent Michot, Anna Stradner, Peter Schurtenberger, and Ruben Kretzschmar. Characterization of the pores in hydrous ferric oxide aggregates formed by freezing and thawing. *Journal of Colloid and Interface Science*, 271(1):163 – 173, 2004.

[119] European Patent Office. Method for producing a sorption material that contains iron, 2001.

[120] Carsten Bahr. *Entfernung von Uran aus Trinkwasser durch Adsorption an Granuliertem Eisenhydroxid (GEH).* PhD thesis, Technische Universität Berlin, 2012.

[121] Barika R. Poole. Point-of-use water treatment for arsenic removal through iron oxide coated sand: Application for the terai region of nepal. Master's thesis, Massachusetts Institute of Technology, 2002.

[122] Luiz C.A. Oliveira, Diego I. Petkowicz, Alessandra Smaniotto, and Sibele B.C. Pergher. Magnetic zeolites: a new adsorbent for removal of metallic contaminants from water. *Water Research*, 38(17):3699 – 3704, 2004.

[123] Georges Tabbal. Technical and social evaluation of three arsenic-removal technologies in nepal. Master's thesis, Massachusetts Institute Of Technology, 2003.